# Exhumation mechanisms of the Tauern Window (Eastern Alps) inferred from apatite and zircon fission track thermochronology

Audrey Bertrand, Claudio Rosenberg, Alain Rabaute, Frédéric Herman, Bernhard Fügenschuh

# Exhumation mechanisms of the Tauern Window (Eastern Alps) inferred from apatite and zircon fission track thermochronology

Audrey Bertrand[1,2] (ID), Claudio Rosenberg[3,4], Alain Rabaute[3,4] (ID), Frédéric Herman[5], and Bernhard Fügenschuh[6]

[1]Department of Tectonics and Sedimentology, Freie Universität Berlin, Berlin, Germany, [2]Now at MTA-ELTE Geological, Geophysical and Space Science Research Group, Budapest, Hungary, [3]ISTeP, UPMC, Sorbonne Universités, Paris, France, [4]CNRS, UMR 7193, Paris, France, [5]Institute of Earth Surface Dynamics, University of Lausanne, Lausanne, Switzerland, [6]Institute of Geology, University of Innsbruck, Innsbruck, Austria

**Abstract** Orogen-parallel extension and orogen-perpendicular shortening accommodated by folding acted at the same time to exhume the Tauern Window. In order to investigate the relative contribution of upright folding and erosion and of extensional denudation for exhumation, we provide compilations in map view of previous and new zircon and apatite fission track ages. These age maps show that isoage contour lines are subparallel to the axial planes of large-scale, upright folds. On age versus distance diagrams, along a profile perpendicular to the dome axis, all thermochronometers show bell-shaped curves with younger ages in the hinge area of the dome and age differences between different chronometers decreasing from the limbs to the hinge area. All these observations suggest that folding synchronous with erosion was largely responsible for exhumation of the Tauern Window. The younger ages and the higher fold amplitudes of the western subdome compared to the eastern one are corroborated by the results of inversion of cooling ages that show higher exhumation rates in the west. These reflect one and the same shortening and folding event that affected the entire Tauern Dome synchronously, but at higher rates than that in the western subdome. Only during Pliocene time were exhumation rates slightly higher along the normal faults bordering the window; hence, extensional unroofing may have dominated exhumation in the Pliocene. The northward displacement of the Dolomites Indenter was associated to a clockwise rotation, which caused increased amounts of shortening westward, hence higher uplift and exhumation rates in the western subdome.

## 1. Introduction

Structural and metamorphic gneiss domes, consisting of large-scale upright folds inside the dome and shear zones along their boundaries, are commonly observed in the cores of orogenic mountain belts [e.g., *Eskola*, 1949; *Crittenden et al.*, 1980] and are inferred to have formed during or after the late stages of collision. Their formation was attributed to different mechanisms, such as diapirism [e.g., *Eskola*, 1949; *Berner et al.*, 1972], tectonic denudation and erosion [e.g., *Coney and Harms*, 1984; *Brun and Van Den Driessche*, 1994], or folding and erosion [e.g., *Ramsay*, 1967; *Burg et al.*, 2004].

Based on the relative orientation of fold axes and of extensional structures, two types of dome have been distinguished: type "a" domes, whose long axis is parallel to the direction of extension and perpendicular to shortening, and type "b" domes, whose long axis is perpendicular to extension [*Jolivet et al.*, 2004]. The majority of "a" domes have axial planes subparallel to the main extensional direction and perpendicular to the low-angle detachment faults bordering the dome [e.g., *Yin*, 1989]. Natural examples of "a-type" domes are the Cenozoic domes in the Alps, i.e., the Tauern [e.g., *Behrmann*, 1988; *Selverstone*, 1988] and Lepontine domes [e.g., *Steck*, 2008], and some of the Aegean core complexes [*Jolivet et al.*, 2004], whereas typical examples of "b-type" domes are the metamorphic core complexes of the North American Cordillera [*Davis and Coney*, 1979].

Whereas extension is unanimously recognized as the main cause of formation and exhumation of b-type domes, the relative roles of shortening and extension in the formation of a-type domes [e.g., *Mancktelow and Pavlis*, 1994] are more difficult to understand. These domes form in different geodynamic settings, going from extensional domains, where the continental crust was severely thinned, as in the Aegean Sea [*Jolivet et al.*, 2004], to collisional settings with thickened crust, as in the Eastern and Central Alps. In the Eastern Alps, the Tauern Window forms an a-type dome that was exhumed during collision. Its internal geometry
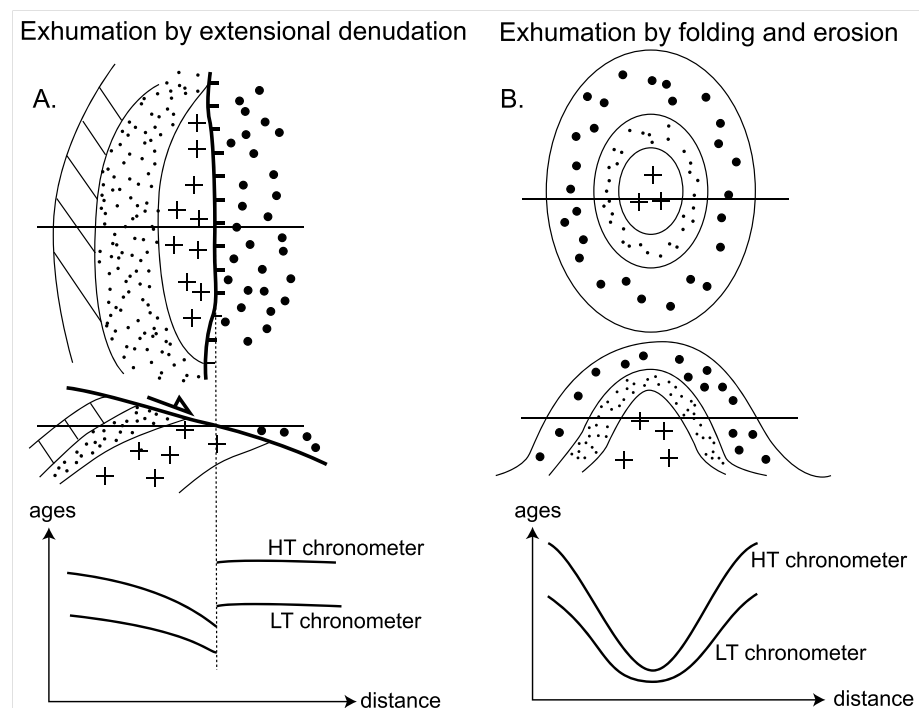
**Figure 1.** Expected age distribution of thermochronometers in map view and cross section in the case of (a) exhumation of a dome related to extensional denudation along a normal fault and (b) doming and exhumation controlled by stationary folding and erosion. Dotted lines indicate expected isoage contour lines. Arrows indicate younging direction of cooling ages. Modified after *Burg et al.* [2004].

is characterized by compressional structures, such as upright folds of >10 km amplitude, and by extensional structures, such as normal faults bordering the eastern and western margins of the dome. As a consequence, the mechanisms inferred to drive exhumation of the Tauern Window span between one end-member model emphasizing the role of folding and erosion [*Cornelius*, 1940; *Laubscher*, 1988; *Lammerer*, 1988; *Rosenberg et al.*, 2004, 2007; *Glodny et al.*, 2008; *Rosenberg and Garcia*, 2011, 2012] and another end-member emphasizing the role of orogen-parallel extensional denudation [*Behrmann*, 1988; *Frisch et al.*, 1998, 2000; *Selverstone*, 1988; *Kuhlemann et al.*, 2001; *Linzer et al.*, 2002; *Scharf et al.*, 2013a]. Although most authors agree that both processes were responsible for the exhumation [*Behrmann*, 1988; *Lammerer*, 1988; *Selverstone*, 1988; *Fügenschuh et al.*, 1997, *Neubauer et al.*, 1999; *Kuhlemann et al.*, 2001; *Linzer et al.*, 2002; *Rosenberg et al.*, 2004, 2007; *Glodny et al.*, 2008; *Rosenberg and Garcia*, 2011, 2012; *Scharf et al.*, 2013a; *Schmid et al.*, 2013], a major question concerns the quantitative assessment of the amount and timing of each of the two mechanisms to the bulk exhumation of the Tauern Window.

The distribution of temperature, hence of cooling ages, within domes varies as a function of their specific exhumation mechanism [e.g., *Burg et al.*, 2004]. For the sake of clarity, two end-member models of exhumation are shown in Figure 1. The first model, in which exhumation only takes place by the activity of large-scale extensional faults, shows that cooling ages are progressively younger from the footwall toward the fault plane [*Wernicke*, 1985; *Foster et al.*, 2001; *Burg et al.*, 2004; *Yin*, 2004; *Brichau et al.*, 2006; *Foster et al.*, 2010]. The second model (Figure 1b), in which exhumation results from folding and synchronous erosion, shows that uplift rates are faster and exhumation is larger along the hinge of the dome, resulting in a symmetrical distribution of cooling ages, younging toward the trace of the axial plane (Figure 1b) [*Burg et al.*, 2004]. Therefore, thermochronological data may help to estimate the distinct contribution of the two processes described above in a gneiss dome like the Tauern Window, where both processes synchronously contributed to its exhumation. We emphasize that Figure 1 illustrates the two end-member models, not their combined effect on the distribution of cooling ages.

In this paper, we focus on fission track data in the Tauern Window and its surroundings. Higher-temperature thermochronometers, as Rb/Sr on biotite and phengite from this Tauern Window area, generally yield
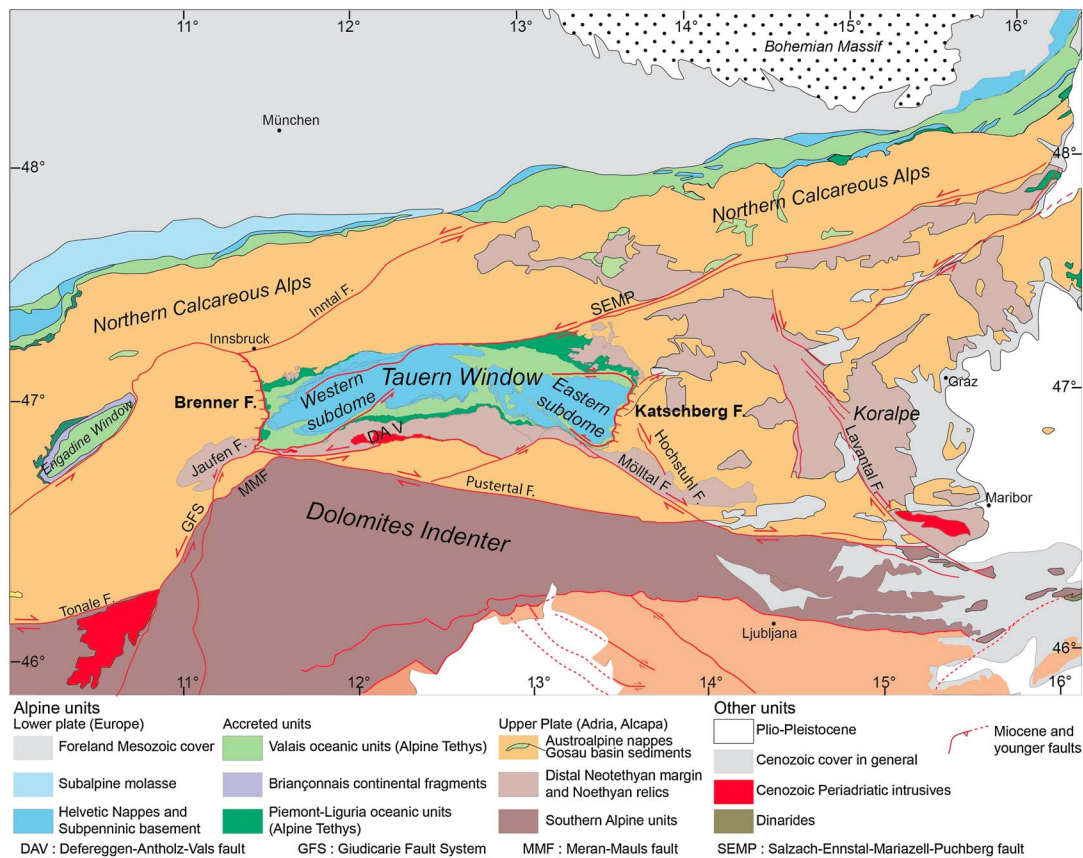
**Figure 2.** Tectonic map of the Eastern Alps [modified after *Handy et al.*, 2010].

formational rather than cooling ages [*Schneider et al.*, 2013]. In addition, the largest number of age data in the Tauern Window and surrounding areas consists of fission track ages. Therefore, the completion of such a database in the central and eastern parts of the Tauern Window will allow us to construct for the first time a reliable pattern of isoage lines from the eastern to western ends of the dome. Assessing whether the age distribution and the cooling history derived from zircon and apatite fission track ages can be related to the first-order structures observed in the Tauern Dome, namely, the large-scale upright folds and the two major extensional faults, will help to interpret the relative contribution of N-S shortening and E-W extension to the exhumation of the Tauern Window.

## 2. Geological Setting

The Tauern Window (Figure 2), located in Austria and northern Italy, is 160 km long and 30 km wide, strikes subparallel to the Eastern Alpine orogen, and exposes a stack of nappes derived from the distal European continental margin and the Alpine Tethyan oceans [*Schmid et al.*, 2013]. The structurally lowest nappes are derived from the European margin, and they form the core of the window (Figure 2).

They consist mainly of orthogneisses ("Zentralgneiss") derived from Variscan granitoids, micaschists, and metavolcanic sediments of the post-Variscan cover. These nappes form the so-called Venediger Duplex [*Lammerer and Weger*, 1998]. An additional nappe derived from the European distal margin lies above this duplex structure. It is the Modereck nappe (Figure 3) that is composed of micaschists, marbles, and quartzites as well as gneisses and amphibolites slivers. Above these units lies the Glockner nappe system [*Schmid et al.*, 2013], derived from the Valais Ocean and mainly composed of calcschists and metapelites intercalated with prasinites, amphibolites, and phyllites. The uppermost nappes of the Tauern Window belong to the Matreier Zone (Figure 3). They are mainly composed of a mélange of ophiolitic mafic rocks and their pelagic cover derived from the Piemont-Liguria Ocean and Permian to Jurassic sediments derived from the Adriatic
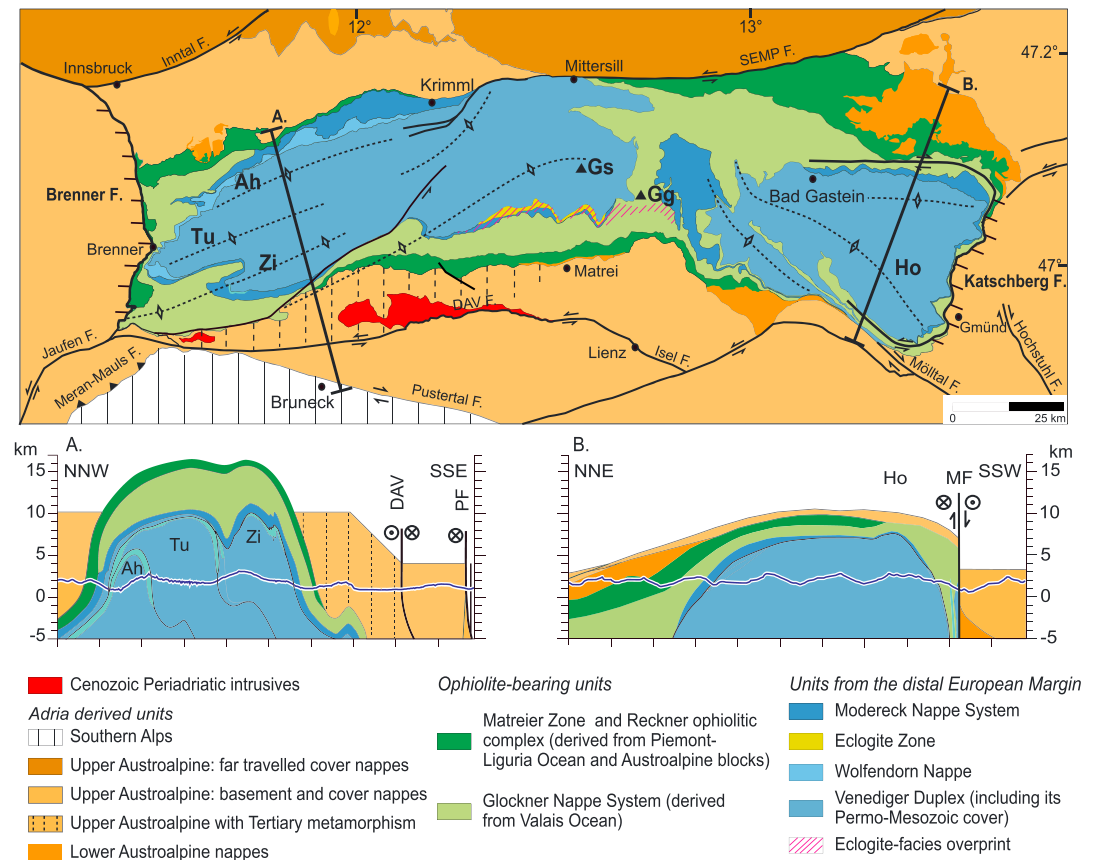
**Figure 3.** Simplified tectonic map of the Tauern Window and cross sections through (a) the western subdome and (b) the eastern subdome [modified after *Schmid et al.*, 2013].

margin [*Schmid et al.*, 2013]. Surrounding the Tauern Window and structurally overlying all the units described above are the Austroalpine nappes (Figure 2), derived from the Adriatic Plate and largely consisting of a metamorphic basement of Variscan age that cooled below 300°C in the Cretaceous (Figure 4). A detailed review of the nappes and lithologies of the Tauern Window is given in *Schmid et al.* [2013].

Upright folding and orogen-parallel extension of the nappe stack described above gave rise to the large-scale dome that forms the Tauern Window (Figure 2). From a structural point of view, the dome can be subdivided into two elongate subdomes. The western one consists of WSW striking, tight upright folds of more than 10 km amplitude (cross-section A, Figure 4), and the eastern one consists of ESE striking folds of lower amplitude and larger wavelength (cross-section B, Figure 4) [*Schmid et al.*, 2013].

Compilation of metamorphic ages in the Alps [*Oberhänsli et al.*, 2004; *Handy and Oberhänsli*, 2004], mainly based on Rb/Sr on biotite, and zircon fission track ages [*Borsi et al.*, 1973, 1978; *Dunkl et al.*, 2003; *Frank et al.*, 1987; *Fügenschuh et al.*, 1997; *Hoinkes et al.*, 1999; *Inger and Cliff*, 1994; *Most*, 2003; *Müller et al.*, 2001; *Reddy et al.*, 1993; *Schuster et al.*, 2004; *Stöckhert*, 1984; *Thöni*, 1999] shows that the European units in the Tauern Window were exhumed through the 250–300°C isotherms, hence through the brittle-ductile transition of basement rocks, mainly during the Miocene, whereas most of the Austroalpine units had already cooled below 300°C in the Cretaceous (Figure 4) [e.g., *Oberhänsli et al.*, 2004; *Handy and Oberhänsli*, 2004]. The area located south of the western Tauern Window and north of the Defereggen-Antholz-Vals (DAV) Fault (Figure 2) is an exception, in that Rb/Sr on biotite ages of these Austroalpine units display Oligocene/Miocene ages [*Borsi et al.*, 1973, 1978]. Therefore, the latter area was included in the so-called Tauern thermal dome [*Frisch et al.*, 2000]. The continuity of cooling ages between this area and the western Tauern Window (Figure 4) is consistent with the continuity of structures observed across this boundary [*Nollau*, 1969], showing tight E-W striking, upright folds in the Austroalpine units that are subparallel to the upright folds of the western Tauern subdome [*Schneider*, 2014].
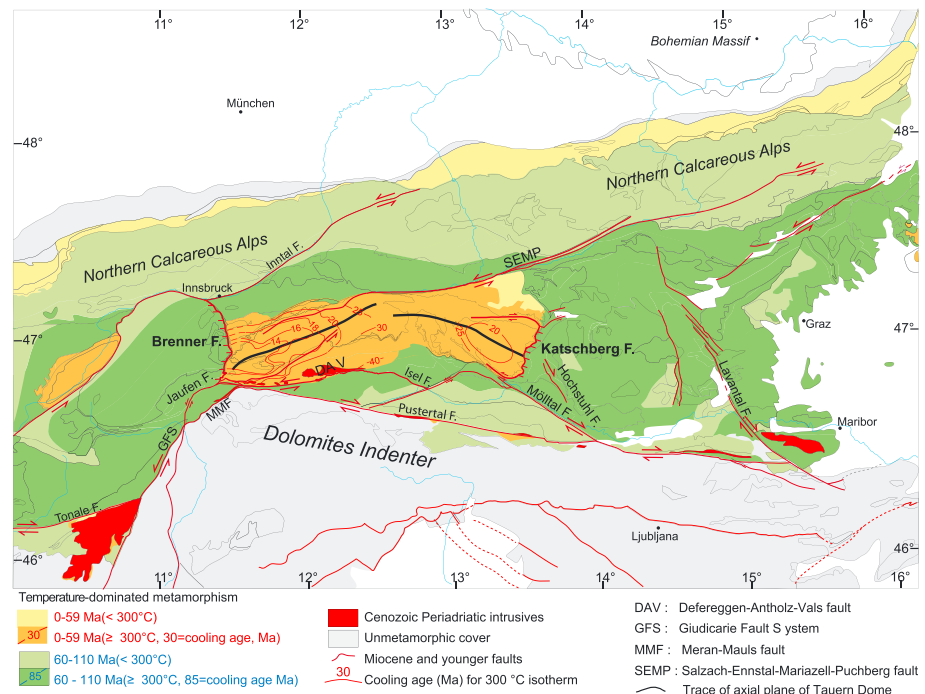
**Figure 4.** Age of temperature-dominated metamorphism in the Eastern Alps [modified after *Handy et al.*, 2010].

Both the western and eastern margins of the window coincide with N-S striking normal faults, the west dipping Brenner Fault [*Behrmann*, 1988; *Selverstone*, 1988] in the west, and the east dipping Katschberg Fault in the east (Figure 3) [*Genser and Neubauer*, 1989; *Scharf et al.*, 2013a]. Based on overprinting relationships between small-scale folds and mylonitic foliations in the footwall of the Brenner, most studies concluded that the normal faults were coeval with the upright folds of the subdomes [*Selverstone*, 1988; *Glodny et al.*, 2008; *Rosenberg and Garcia*, 2011, 2012; *Fügenschuh et al.*, 2012; *Scharf et al.*, 2013a; *Schmid et al.*, 2013]. However, the amount of extensional displacement accommodated by the normal faults, and in particular by the Brenner Fault, remains a matter of debate [*Rosenberg and Garcia*, 2011, 2012; *Fügenschuh et al.*, 2012]. Estimates vary from a maximum value of >40 km [*Fügenschuh et al.*, 2012] to as little as 4–14 km [*Rosenberg and Garcia*, 2011]. The first interpretation relies on the inferred vertical offset of 17 km along the Brenner Fault. Assuming that this offset resulted from extension and assuming that the present-day mylonites have the same orientation of the shear plane during extension, the latter offset results in >40 km of extensional displacement [*Fügenschuh et al.*, 2012]. The second interpretation considers that the >10 km amplitude of the eroded upright folds accounts for >10 km of the vertical offset across the Brenner Fault [*Rosenberg and Garcia*, 2011, 2012]. Hence, only 7 km of vertical offset needs to be accommodated by extension along the Brenner Fault.

Estimates of extension along the Katschberg Fault vary between 17.3 km [*Genser and Neubauer*, 1989] and 23–29 km [*Scharf et al.*, 2013a]. The first estimate was based on the inferred difference of 300°C in the metamorphic T between the footwall and hanging wall. This gap was interpreted to result from a vertical offset of 10 km, by assuming a geothermal gradient of 30°C/km. Resolving this vertical offset on a fault plane dipping 30° to the east resulted in 17.3 km of horizontal displacement [*Genser and Neubauer*, 1989]. The second interpretation relies on the vertical offset of 13.5 km measured on a cross section striking perpendicular to the Katschberg Fault. Resolving this vertical offset on a fault plane inferred to dip 25–30° yields a horizontal displacement of 23–29 km [*Scharf et al.*, 2013a].

Large parts of the northern and southern margins of the Tauern Window are defined by strike-slip faults. In the north, the almost 400 km long, E to ENE striking, sinistral SEMP (Salzach-Ennstal-Mariazell-Puchberg) Fault (Figure 2) [*Decker and Peresson*, 1996] accommodated a lateral offset of 60–70 km [*Linzer et al.*, 1995]. Based on the age of deformed and dated conglomerates within pull-apart basins along the SEMP [*Steininger et al.*, 1989], its activity is inferred to be Miocene [17 Ma; *Peresson and Decker*, 1997]. At its western termination, the
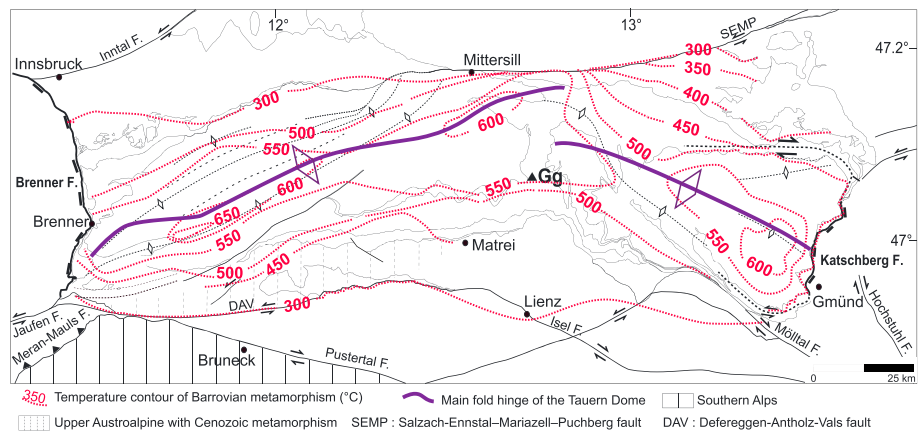
**Figure 5.** Simplified tectonic map of the Tauern Window showing isograds of Barrovian metamorphism. Isograds in the central and western areas are based on oxygen thermometry on quartz-muscovite [*Hoernes and Friedrichsen*, 1974]; isograds in the Grossglockner (Gg) and eastern areas are based on Raman microspectrometry of carbonaceous material [*Scharf et al.*, 2013a, 2013b]. The 300°C isograd south of the Tauern Window is drawn along the boundary between Oligocene/Miocene and Cretaceous Rb/Sr biotite ages [*Borsi et al.*, 1973, 1978]. This boundary coincides with the DAV Fault in the west and with the limit between Cenozoic and Mesozoic zircon fission track ages further east [*Dunkl et al.*, 2003; *Wölfler et al.*, 2008; *Steenken et al.*, 2002; *Most*, 2003; *Fügenschuh et al.*, 1997]. The purple line is the trace of the axial plane of the Tauern Dome.

SEMP Fault bends into the interior of the Tauern Window (Figure 3), where sinistral displacement is transferred into N-S shortening [*Rosenberg and Schneider*, 2008]. In the south, the sinistral transpressive DAV (Defereggen-Antholz-Vals) Fault (Figures 2 and 3) [*Kleinschrodt*, 1987] coincides with the southern limit of Cenozoic Alpine metamorphism [*Hoinkes et al.*, 1999], hence the southern limit of the Tauern thermal dome (Figure 4). Both the SEMP and the DAV belong to a set of large-scale, sinistral faults inferred to be coeval and conjugate to dextral faults located south and east of the Tauern Window (Figure 2). The combined activity of all these faults resulted in the east directed lateral extrusion of the orogenic wedge in front of the Dolomites Indenter [*Ratschbacher et al.*, 1991].

The Cenozoic metamorphic history of the Tauern Window started with Eo-Oligocene subduction of the oceanic-derived units and the distal European margin [*Schmid et al.*, 2013] below the (Austroalpine) Adriatic Plate. This phase was followed by a Barrow-type metamorphism [e.g., *Bousquet et al.*, 2008], whose peak is inferred to have been attained between 30 and 28 Ma [*Reddy et al.*, 1993; *Selverstone et al.*, 1992; *Christensen et al.*, 1994; *Inger and Cliff*, 1994; *Thöni*, 1999] or 34 and 30 Ma [*Schneider et al.*, 2015]. Cooling and exhumation followed the peak of metamorphism from early Oligocene to late Miocene [e.g., *Hoinkes et al.*, 1999; *Handy and Oberhänsli*, 2004]. In contrast, the Austroalpine units were not affected by any of these two metamorphic events, being part of the brittle lid of the orogen throughout the Cenozoic time.

The isograds of Barrovian metamorphism are subparallel to and symmetrically distributed about the fold axial plane of the dome (Figure 5), with metamorphic T increasing toward the core of each subdome (Figure 5). Therefore, either the isograds are coeval to the dome formation or they are older and were folded during upright folding. However, since they crosscut the nappe contacts (Figure 5), they postdate nappe formation that occurred during Paleocene and Eocene times [*Selverstone*, 1985; *Genser et al.*, 1996; *Bousquet et al.*, 2008; *Schmid et al.*, 2013; *Scharf et al.*, 2013b]. Doming by upright folding is inferred to have been active since 28 Ma, as indicated by dating of syncrenulation allanite porphyroblasts [*Cliff et al.*, 2015]. A similar age range was suggested for the initiation of the Brenner normal fault [*Selverstone*, 1988; *Christensen et al.*, 1994; *Axen et al.*, 1995].

Physical, analogue models that investigated deformation of an analogue lithosphere due to indentation of a rigid body with the shape of the Dolomites Indenter showed the formation of orogen-parallel, upright folds and thrusts in front of the indenter tip and its surroundings [*Ratschbacher et al.*, 1991; *Rosenberg et al.*, 2004; 2007]. Models testing different convergence directions showed that NNE directed convergence induced a deformation pattern very similar to that presently observed in front of the Dolomites Indenter [*Rosenberg et al.*, 2007]. Based on these results, it was suggested that Dolomites' indentation caused a series of faults

and folds whose erosion could explain the formation and exhumation of the Tauern Window [*Rosenberg et al.*, 2004]. In contrast, based on 2-D palinspastic reconstructions [*Frisch et al.*, 1998, 2000], the dominating process shaping and exhuming the Tauern Dome during Cenozoic times was suggested to be orogen-parallel extension. In spite of the large-scale compressive, collisional setting, these models emphasized the role of lateral extrusion associated to orogen-parallel extension, hence extensional denudation as a major mechanism for exhumation [*Genser and Neubauer*, 1989; *Axen et al.*, 1995; *Wang and Neubauer*, 1998; *Neubauer et al.*, 1999; *Fügenschuh et al.*, 1997; *Kuhlemann et al.*, 2001; *Linzer et al.*, 2002]. In this context, extension of the upper crust would be accommodated, within the Tauern Window, by normal faulting along the Brenner and Katschberg Faults [*Selverstone*, 1988; *Behrmann*, 1988; *Genser and Neubauer*, 1989; *Axen et al.*, 1995; *Frisch et al.*, 1998; *Wang and Neubauer*, 1998; *Neubauer et al.*, 1999, 2000; *Kuhlemann et al.*, 2001; *Linzer et al.*, 2002].

Alternative models [*Genser and Neubauer*, 1989; *Neubauer et al.*, 1999] also proposed that exhumation of the Tauern Window was driven by major extension along the Brenner and Katschberg Faults but considered these structures as part of a sinistral transtensive system, defined by the SEMP Fault in the north and the DAV Fault in the south (Figure 2). Exhumation of the Tauern Window was thereby interpreted as a pull-apart structure, formed during ESE-WNW stretching [*Genser and Neubauer*, 1989].

## 3. Analytical Procedures

Mineral separation followed standard procedures as described by *Donelik et al.* [2005]. Apatites and zircons were then mounted in epoxy and Teflon, respectively, and polished. Revelation of spontaneous tracks was done in 6.5% nitric acid for 40 s at 20°C for the apatites and in a NaOH-KOH eutectic melt for 3–8 h at 235°C for the zircons. Irradiation of both zircons and apatites was carried out at the Forschungsreaktor München II research reactor in Garching, Germany. The neutron flux was monitored using CN1 (for zircon) and CN5 (for apatite) dosimeter glasses. Induced tracks in the external detector muscovite were etched in 40% hydrogen fluoride for 45 min at 20°C. All samples were analyzed using the external detector method as described by *Gleadow* [1981], and measurements were carried out using a Zeiss Axio Imager A1m microscope equipped with an AutoScan™ stage. Ages were calculated using the zeta calibration approach [*Hurford and Green*, 1983] with a zeta factor of $\zeta_{CN-1} = 189.0 \pm 11.1$ (zircon, CN1 glass) and $\zeta_{CN-5} = 338.9 \pm 33.3$ (apatite, CN5 glass) and the software Trackkey® [*Dunkl*, 2002], with errors quoted at 2σ.

Fission track ages represent the time when crystals cooled below the partial annealing zone (PAZ), defined by a temperature range in which early-formed tracks can partially anneal. The healing capacity of fission tracks depends, among others, on the time, the chemical composition of the crystal, and the total accumulated radiation damage [*Gleadow and Duddy*, 1982; *Kasuya and Naeser*, 1988]. Therefore, the temperature of the PAZ range between 60°C and 120°C for apatite [*Green et al.*, 1989] and between 180°C and 300°C for the zircon [*Hurford and Green*, 1983]. The annealing kinetics of fission tracks in zircon depends in particular on the presence of radiation damage in the crystal [*Kasuya and Naeser*, 1988]. In high-retention zircon crystals, with no or little radiation damage, fission tracks are annealed at temperatures of ~280–300°C [*Garver et al.*, 2005], whereas in low-retention zircon crystals, with higher radiation damage, fission tracks are annealed at temperatures of ~180–200°C [*Garver et al.*, 2005]. Therefore, the mean closure temperature of zircon fission tracks is currently estimated at 240 ± 60°C [*Yamada et al.*, 1995]. The annealing kinetics of fission tracks in apatite depend in particular on the ratio between chlorine and fluorine contents [*Gleadow and Duddy*, 1982; *Green et al.*, 1985, 1986; *O'Sullivan and Parrish*, 1995], which is estimated by measuring the length of etch pits parallel to the crystallographic c axis, the Dpar [*Donelick*, 1993]. If Dpar is <1.75 μm, apatite crystals most likely are richer in fluorine, whereas if Dpar > 1.75 μm, apatites are considered to be richer in chlorine [*Donelik et al.*, 2005]. Fission tracks in chlorapatite are more resistant to annealing than in fluorapatite [*Green et al.*, 1989; *Crowley et al.*, 1991; *Donelick et al.*, 1999]. Cl apatite crystals anneal at ~130 ± 10°C [*O'Sullivan and Parrish*, 1995] whereas F-rich apatites anneal at 110 ± 20°C [*Green et al.*, 1986].

## 4. Results

### 4.1. New Zircon and Apatite Fission Track Ages

As shown by previous compilations of fission track ages from the Tauern Window [*Luth and Willingshofer*, 2008; *Rosenberg and Berger*, 2009], some areas were poorly covered, making it difficult to interpret the age
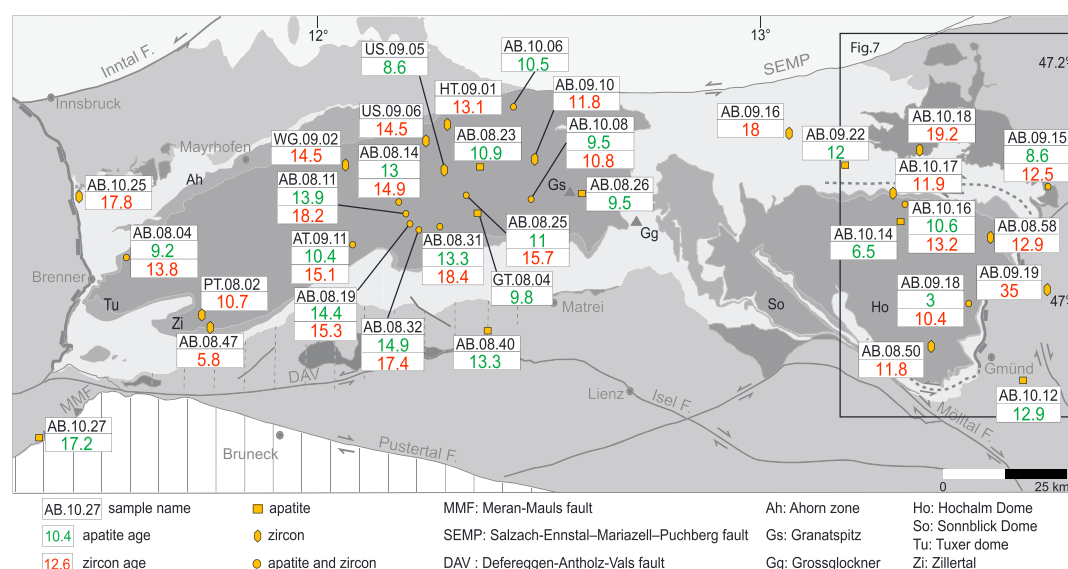
**Figure 6.** Tectonic map of the Tauern Window showing locations and age of new fission track samples. The rectangle shows the location of Figure 7.

distribution over the whole region. Twenty-two new apatite and 25 new zircon fission track ages were produced for this study (Figure 6, Table I).

Zircon fission track ages range between 5.8 ± 0.8 Ma in the southwestern part of the Tauern Window (sample AB.08.47, Figure 6) and 35 ± 4.2 Ma in the hanging wall of the Katschberg Fault (sample AB.09.19, Figure 6). Ages obtained for the western subdome vary between 13.1 ± 1.6 and 18.4 ± 2.2 Ma, an age range similar to that of previous studies (between 11 and 22 Ma) [*Most*, 2003]. In the core of the Tauern Window, i.e., in the Granatspitz area (Figure 6), zircon fission track ages vary between 10.8 ± 1.4 and 11.8 ± 1.4 Ma. These ages are younger than those found in the eastern and western subdomes (Figure 6).

In the eastern subdome, zircon ages vary between 10.4 ± 2.1 and 19.2 ± 2.3 Ma (Figure 6). Within the Hochalm dome, fission track ages are distributed within a narrower time interval, namely, between 10.4 ± 2.1 and 13.2 ± 1.5 Ma. These ages are significantly younger than those previously published for the same area (between 18 and 16 Ma; Figure 7) [*Dunkl et al.*, 2003]. Even where samples were collected very close to those of *Dunkl et al.* [2003] (Figure 7), an age difference of 5 Ma exists. This disparity is not due to different elevations of the samples (Table I), nor to the vicinity to the Katschberg Fault (Figure 7). As shown by radial plots (Figure 7), the distributions of zircon ages in the Hochalm dome show that both sets of data [*Dunkl et al.*, 2003; this study] are characterized by a wide distribution of single-grain ages that largely overlap and range between 5.9 and 28.4 Ma in the case of this study and between 8.4 and 31 Ma in *Dunkl et al.* [2003]. Because three of our samples are based on a small number (five to six) of zircon grains (Figure 7), we do not include them in the map interpolation (Figure 8), only relying on those of *Dunkl et al.* [2003] for the easternmost termination of the Tauern Window.

Mean Dpar values of the tracks in apatites range from 1.2 to 1.72 μm (Table I), indicating fluorapatite composition. Therefore, the annealing kinetics of the apatite crystals are considered similar and their closure temperature can be inferred to correspond to 110 ± 20°C [*Green et al.*, 1986]. Apatite ages vary between 17.2 ± 2.4 Ma in the Austroalpine units, along the Meran-Mauls Fault, and 3 ± 0.4 Ma in the footwall of the Katschberg Fault (Figure 6). This may indicate that the Katschberg Fault was still active in the Pliocene. However, given the age gap between the latter sample and the neighboring ones (Figure 6), a local age reset due to late, thermal fluid circulation, whose temperature was sufficiently high to anneal apatite fission tracks, may be more likely. Zircon fission track ages from the same sample also provide younger ages (10.4 ± 2.1 Ma) than the neighboring samples (16.7 ± 1 and 17.1 ± 1.3 Ma), suggesting that fluids may have partially reset the fission tracks in the zircon crystals too. In the Granatspitz area, ages are slightly younger when compared to the western subdome (Figure 6). Taken together, the data are consistent with ages previously obtained in

**Table I.** New Zircon and Apatite Fission Track Ages[a]

| Sample | Long. (DDEC) | Lat. (DDEC) | Z (m) | Unit | Lithology | Apatite | | | | | | | Zircon | | | | | |
|---|---|---|---|---|---|---|---|---|---|---|---|---|---|---|---|---|---|---|
| | | | | | | Nb of Crystals | $\rho_D$ (105 cm$^{-2}$) | $\rho_s$ (105 cm$^{-2}$) | $\rho_i$ (105 cm$^{-2}$) | Dpar (μm) | χ (%) | Central Age ±1σ (Ma) | Nb of Crystals | $\rho_D$ (105 cm$^{-2}$) | $\rho_s$ (105 cm$^{-2}$) | $\rho_i$ (105 cm$^{-2}$) | χ (%) | Central Age ±1σ (Ma) |
| AB.08.04 | 11.5845 | 47.0389 | 1400 | Zgneiss | granitgneiss | 14 | 1.38 | 0.13 | 3.13 | 1.22 | 62.19 | 9.2 ± 1.5 | 13 | 0.50 | 2.57 | 9.09 | 0.0 | 13.8 ± 1.9 |
| AB.08.11 | 12.2510 | 47.1003 | 2671 | Zgneiss | paragneiss | 15 | 1.33 | 0.12 | 1.97 | 1.64 | 99.64 | 13.9 ± 2.4 | 17 | 0.50 | 2.45 | 6.30 | 95.98 | 18.2 ± 2.1 |
| AB.08.14 | 12.2358 | 47.1102 | 2754 | Zgneiss | paragneiss | 8 | 0.99 | 0.12 | 1.53 | 1.72 | 92.91 | 13.0 ± 2.8 | 5 | 0.50 | 1.91 | 6.07 | 78.79 | 14.9 ± 2.0 |
| AB.08.19 | 12.2683 | 47.0967 | 2730 | Zgneiss | paragneiss | 20 | 1.28 | 0.23 | 3.38 | 1.32 | 95.08 | 14.4 ± 1.7 | 16 | 0.49 | 3.29 | 9.91 | 0.0 | 15.3 ± 1.9 |
| AB.08.23 | 12.4259 | 47.1580 | 2294 | Zgneiss | paragneiss | 20 | 0.97 | 0.21 | 3.04 | 1.40 | 89.29 | 10.9 ± 1.3 | - | - | - | - | - | - |
| AB.08.25 | 12.3922 | 47.1198 | 2832 | Zgneiss | granitgneiss | 7 | 0.95 | 0.11 | 1.67 | - | 98.2 | 11.0 ± 2.7 | 21 | 0.52 | 2.04 | 6.31 | 53.56 | 15.7 ± 1.8 |
| AB.08.26 | 12.6248 | 47.1164 | 2462 | Zgneiss | granitgneiss | 12 | 1.23 | 0.23 | 4.92 | 1.20 | 75.57 | 9.5 ± 1.4 | - | - | - | - | - | - |
| AB.08.31 | 12.3314 | 47.0852 | 2500 | Zgneiss | paragneiss | 21 | 1.37 | 0.11 | 1.91 | 1.47 | 99.98 | 13.3 ± 2.1 | 20 | 0.52 | 3.15 | 8.48 | 0.02 | 18.4 ± 2.2 |
| AB.08.32 | 12.2484 | 47.0885 | 2547 | Zgneiss | paragneiss | 10 | 0.92 | 0.16 | 1.66 | - | 69.16 | 14.9 ± 2.7 | 19 | 0.41 | 2.84 | 6.38 | 32.95 | 17.4 ± 2.0 |
| AB.08.40 | 12.3847 | 46.9425 | 2618 | Zgneiss | greenschist | 20 | 0.91 | 0.20 | 2.22 | 1.33 | 99.94 | 13.3 ± 1.7 | - | - | - | - | - | - |
| AB.08.47 | 11.7409 | 46.9406 | 2655 | Zgneiss | paragneiss | - | - | - | - | - | - | - | 8 | 0.22 | 1.95 | 6.84 | 12.32 | 5.8 ± 0.8 |
| AB.08.50 | 13.4043 | 46.8928 | 1939 | Zgneiss | paragneiss | - | - | - | - | - | - | - | 6 | 0.24 | 5.93 | 11.55 | 4.04 | 11.8 ± 1.6 |
| AB.08.58 | 13.5664 | 47.0800 | 1095 | Zgneiss | granitgneiss | - | - | - | - | - | - | - | 6 | 0.42 | 1.91 | 6.84 | 10.03 | 12.9 ± 1.8 |
| AB.09.10 | 12.5315 | 47.1761 | 1473 | Zgneiss | granitgneiss | - | - | - | - | - | - | - | 9 | 0.25 | 5.61 | 10.95 | 0.23 | 11.8 ± 1.4 |
| AB.09.15 | 13.6807 | 47.1406 | 1196 | AA | granitgneiss | 4 | 1.15 | 0.21 | 4.63 | - | 82.22 | 8.6 ± 2.3 | 2 | 0.41 | 2.49 | 7.48 | 58.47 | 12.5 ± 2.1 |
| AB.09.16 | 13.1151 | 47.2177 | 906 | Glockner | greenschist | - | - | - | - | - | - | - | 2 | 0.42 | 2.64 | 5.87 | 2.68 | 18.0 ± 2.1 |
| AB.09.18 | 13.4874 | 46.9681 | 1008 | Zgneiss | migmatite | 20 | 0.29 | 0.14 | 2.17 | 1.39 | 94.45 | 3.0 ± 0.4 | 6 | 0.26 | 4.23 | 10.80 | 0.02 | 10.4 ± 2.1 |
| AB.09.19 | 13.6162 | 46.9931 | 1196 | AA | phyllite | - | - | - | - | - | - | - | 8 | 0.41 | 5.11 | 5.61 | 86.1 | 35.0 ± 4.2 |
| AB.09.22 | 13.2893 | 47.1449 | 1160 | Glockner | greenschist | 6 | 0.98 | 0.32 | 1.78 | - | 97.37 | 12.0 ± 2.8 | - | - | - | - | - | - |
| AB.10.06 | 12.4898 | 47.2340 | 1014 | Zgneiss | diorite | 18 | 1.02 | 0.24 | 3.77 | 1.40 | 43.07 | 10.5 ± 1.3 | - | - | - | - | - | - |
| AB.10.08 | 12.5050 | 47.1022 | 1523 | Zgneiss | aplitic gneiss | 16 | 1.02 | 0.15 | 2.63 | 1.26 | 97.17 | 9.5 ± 1.4 | 12 | 0.29 | 6.05 | 15.40 | 0.0 | 10.8 ± 1.4 |
| AB.10.12 | 13.5364 | 46.8617 | 1440 | AA | orthogneiss | 20 | 1.03 | 0.34 | 4.49 | 1.27 | 80.45 | 12.9 ± 1.4 | - | - | - | - | - | - |
| AB.10.14 | 13.3462 | 47.0844 | 1940 | Zgneiss | granitgneiss | 21 | 1.05 | 0.19 | 5.06 | 1.32 | 90.98 | 6.5 ± 0.8 | - | - | - | - | - | - |
| AB.10.16 | 13.3513 | 47.1148 | 2405 | Zgneiss | granitgneiss | 14 | 1.05 | 0.16 | 2.76 | 1.37 | 78.26 | 10.6 ± 1.4 | 12 | 0.32 | 4.59 | 10.38 | 29.97 | 13.2 ± 1.5 |
| AB.10.17 | 13.3441 | 47.1316 | 2030 | Glockner | granitgneiss | - | - | - | - | - | - | - | 16 | 0.33 | 3.96 | 10.04 | 0.08 | 11.9 ± 1.4 |
| AB.10.18 | 13.3622 | 47.1975 | 2000 | AA | quartzite | - | - | - | - | - | - | - | 16 | 0.34 | 0.69 | 1.19 | 0.29 | 19.2 ± 2.3 |
| AB.10.25 | 11.4641 | 47.1294 | 1171 | Zgneiss | quartzite | - | - | - | - | - | - | - | 14 | 0.35 | 2.88 | 5.35 | 0.0 | 17.8 ± 2.2 |
| AB.10.27 | 11.4409 | 46.7973 | 1557 | AA | granite | 14 | 1.07 | 0.17 | 1.73 | 1.72 | 99.13 | 17.2 ± 2.4 | - | - | - | - | - | - |
| AT.09.11 | 12.1361 | 47.0741 | 2645 | Zgneiss | tonalit gneiss | 16 | 1.08 | 0.14 | 2.46 | 1.41 | 93.07 | 10.4 ± 1.4 | 9 | 0.37 | 2.87 | 6.59 | 1.08 | 15.1 ± 1.9 |
| GT.08.04 | 12.4103 | 47.0832 | 2783 | Zgneiss | aplitic gneiss | 20 | 1.09 | 0.17 | 3.12 | 1.37 | 83.86 | 9.8 ± 1.2 | - | - | - | - | - | - |
| HT.09.01 | 12.3468 | 47.2176 | 1317 | Zgneiss | tonalit gneiss | - | - | - | - | - | - | - | 20 | 0.39 | 3.79 | 10.41 | 0.0 | 13.1 ± 1.6 |
| PT.08.02B | 11.7247 | 46.9647 | 2825 | Zgneiss | tonalit gneiss | - | - | - | - | - | - | - | 2 | 0.40 | 4.01 | 13.68 | 53.54 | 10.7 ± 1.5 |
| US.09.05 | 12.3293 | 47.1535 | 2174 | Zgneiss | tonalit gneiss | 15 | 1.10 | 0.12 | 2.54 | 1.55 | 96.7 | 8.6 ± 1.3 | - | - | - | - | - | - |
| US.09.06 | 12.2933 | 47.1934 | 1375 | Zgneiss | tonalit gneiss | - | - | - | - | - | - | - | 19 | 0.40 | 5.12 | 12.85 | 6.42 | 14.5 ± 1.7 |
| WG.09.02 | 12.1214 | 47.1571 | 2429 | Zgneiss | tonalit gneiss | - | - | - | - | - | - | - | 18 | 0.43 | 4.15 | 11.29 | 0.0 | 14.5 ± 1.7 |

[a]$\rho_D$: track density of the dosimeter glass; $\rho_s$: spontaneous track density; $\rho_i$: induced track density; χ: chi-square statistics. Apatite ages are calculated using $\zeta_{CN-5}$ = 338.9 ± 33.3. Zircon ages are calculated using $\zeta_{CN-1}$ = 189.0 ± 11.1. GN: Glockner nappe, LAA: lower Austroalpine units, MN: Modereck nappe, MZ: Matreier Zone, UAA: upper Austroalpine units, VD: Venediger Duplex.
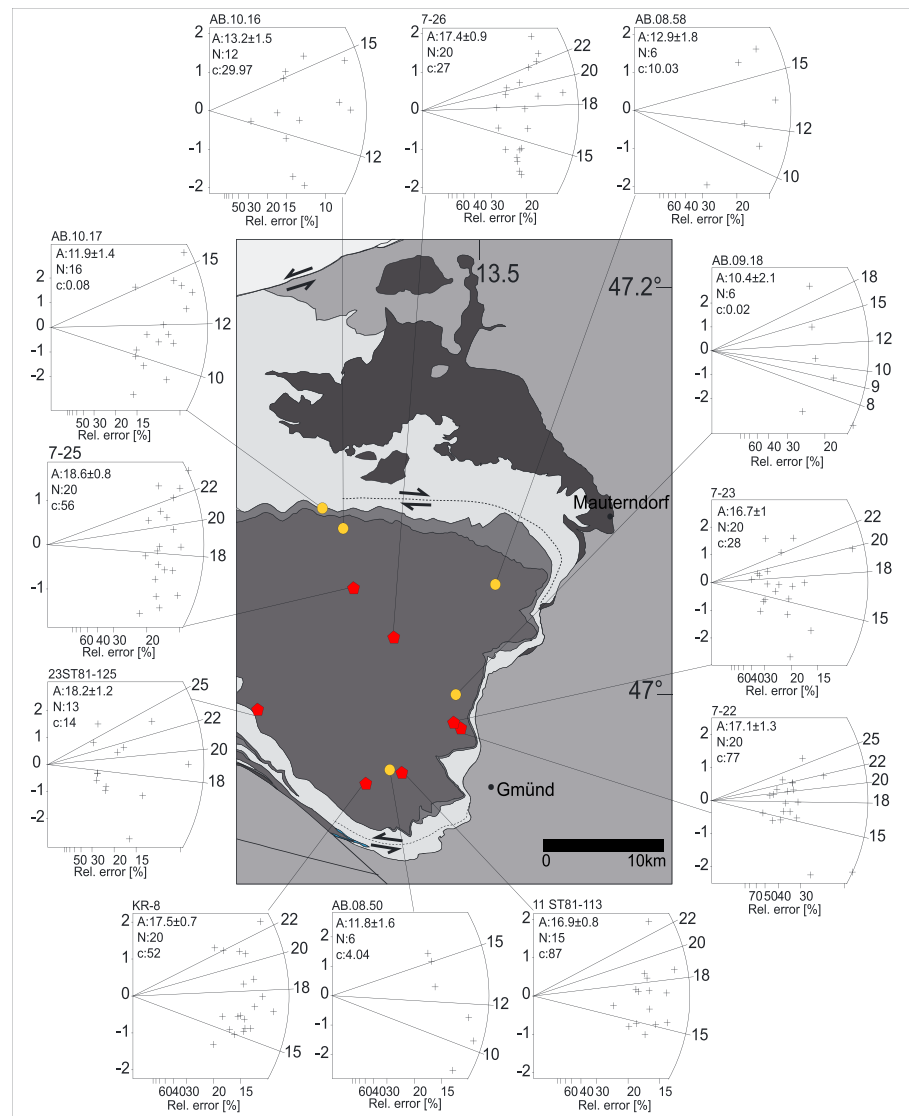
**Figure 7.** Radial plots showing the wide single-grain range of zircon fission track ages in the Hochalm Dome. Red pentagons are from *Dunkl et al.* [2003] and yellow circles from this study. A: central zircon fission track age; N: number of crystals counted; $\chi$: $\chi^2$ statistical hypothesis test; left ordinate axis: $\sigma$ error; right ordinate axis: timescale (Ma); abscissa axis: relative error.

neighboring areas of the Tauern Window and allow one to explore along-strike variations in fission track ages along the entire Tauern Window.

### 4.2. Isoage Maps

Our new data and all available zircon and apatite fission track ages from the Tauern Window and surrounding Austroalpine areas [*Grundmann and Morteani*, 1985; *Staufenberg*, 1987; *Coyle*, 1994; *Fügenschuh et al.*, 1997; *Mancktelow et al.*, 2001; *Viola et al.*, 2001; *Steenken et al.*, 2002; *Dunkl et al.*, 2003; *Most*, 2003; *Foeken et al.*, 2007; *Pomella*, 2010; *Wölfler et al.*, 2008, 2012, 2015; *Di Fiore*, 2013] are compiled and interpolated using a natural neighbor algorithm tool of Esri ArcMap 10™ geographic information system (GIS) software (Figures 8b and 9b). Extended cells for the interpolation are of 500 m, and analytical errors are not taken into account. Age classes of the interpolated maps are identical for all data sets, and they are based on the analysis of the distribution histograms of zircon and apatite fission track ages.

The Tauern thermal dome coincides quite well with zircon ages younger than 22–24 Ma (Figure 8). However, the area bounded by the Jaufen and Meran-Mauls Faults also displays ages ranging between 14 and 19 Ma
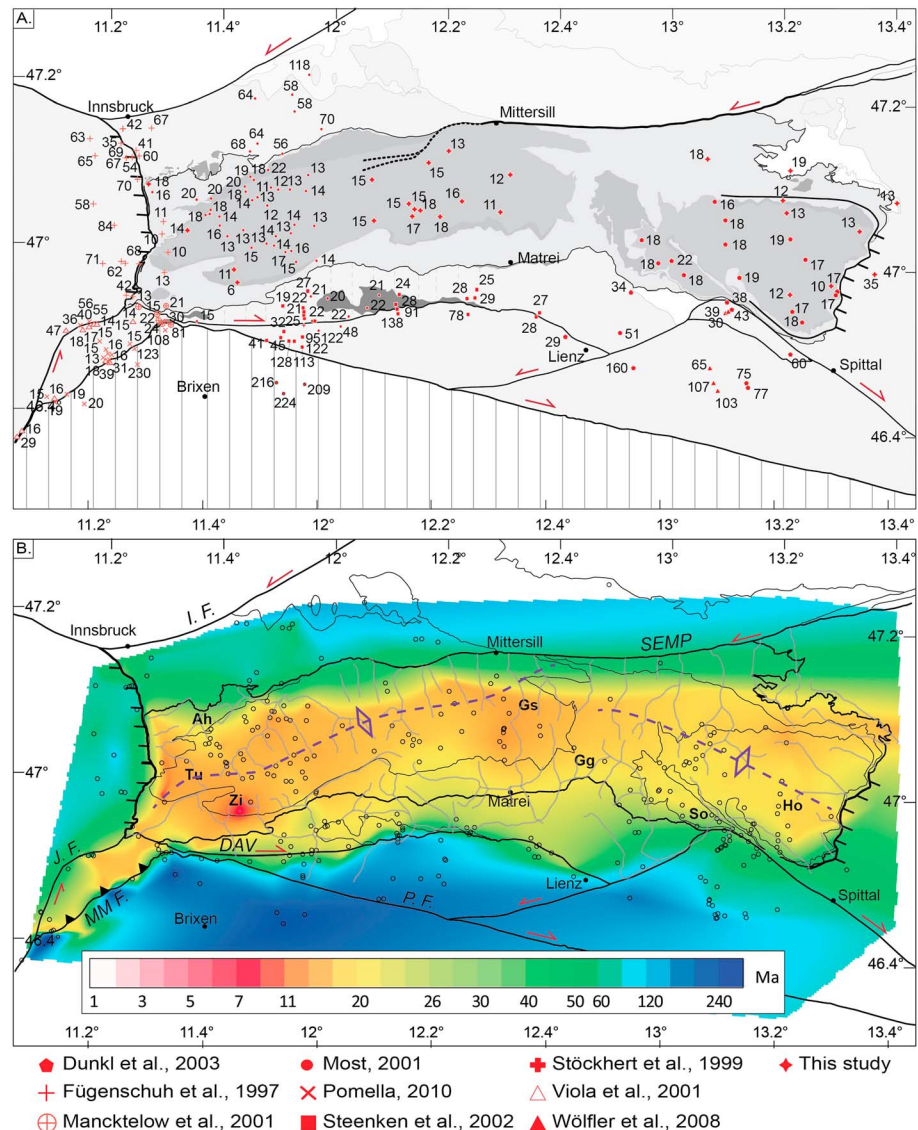
**Figure 8.** Distribution of compiled and new zircon fission track ages. (a) Sample ages in Ma. (b) Interpolation of ages using the natural neighbor algorithm provided by Esri ArcMap 10™ GIS software. Dashed, purple lines: trace of axial plane of Tauern Dome. BF: Brenner Fault; DAV: Defereggen-Antholz-Vals Fault; J.F.: Jaufen Fault; MM F. Meran-Mauls Fault; KF: Katschberg Fault; P.F.: Periadriatic Fault; SEMP: Salzach-Ennstal-Mariazell-Puchberg Fault; Gg: Grossglockner; Gs: Granatspitz; Ho: Hochalm Dome; So: Sonnblick Dome.

(Figure 8). Therefore, from a thermal point of view, this area represents the southwestern continuation of the Tauern Window. Zircon ages become younger toward the core of the western subdome (Figures 8 and 10), and the area covered by the youngest ages (<14 Ma) strikes ESE, subparallel to the isograds (Figure 5) and to the axial plane of the dome. In the eastern subdome, zircon ages are more evenly distributed (Figure 8) and isograds are more distant to each other (Figure 5).

A large age gap coincides with the Brenner Fault, separating Miocene zircon ages in the footwall from Cretaceous ages in the hanging wall (Figure 8) [*Fügenschuh et al.*, 1997]. A similar age jump is observed across the Jaufen Fault (Figure 8). In the area located between the Jaufen and Meran-Mauls Faults, ages cluster between 12.9 ± 1.3 Ma [*Pomella*, 2010] and 19.3 ± 1 Ma [*Viola et al.*, 2001], whereas north of the Jaufen Fault they are older than 29 ± 5.2 Ma [*Viola et al.*, 2001]. Within large parts of the eastern subdome, zircon ages show only small variations (Figure 8), most ages varying between 20 and 15 Ma, and only along its margin, in the immediate footwall of the Katschberg normal fault, do ages become younger (Figure 8).
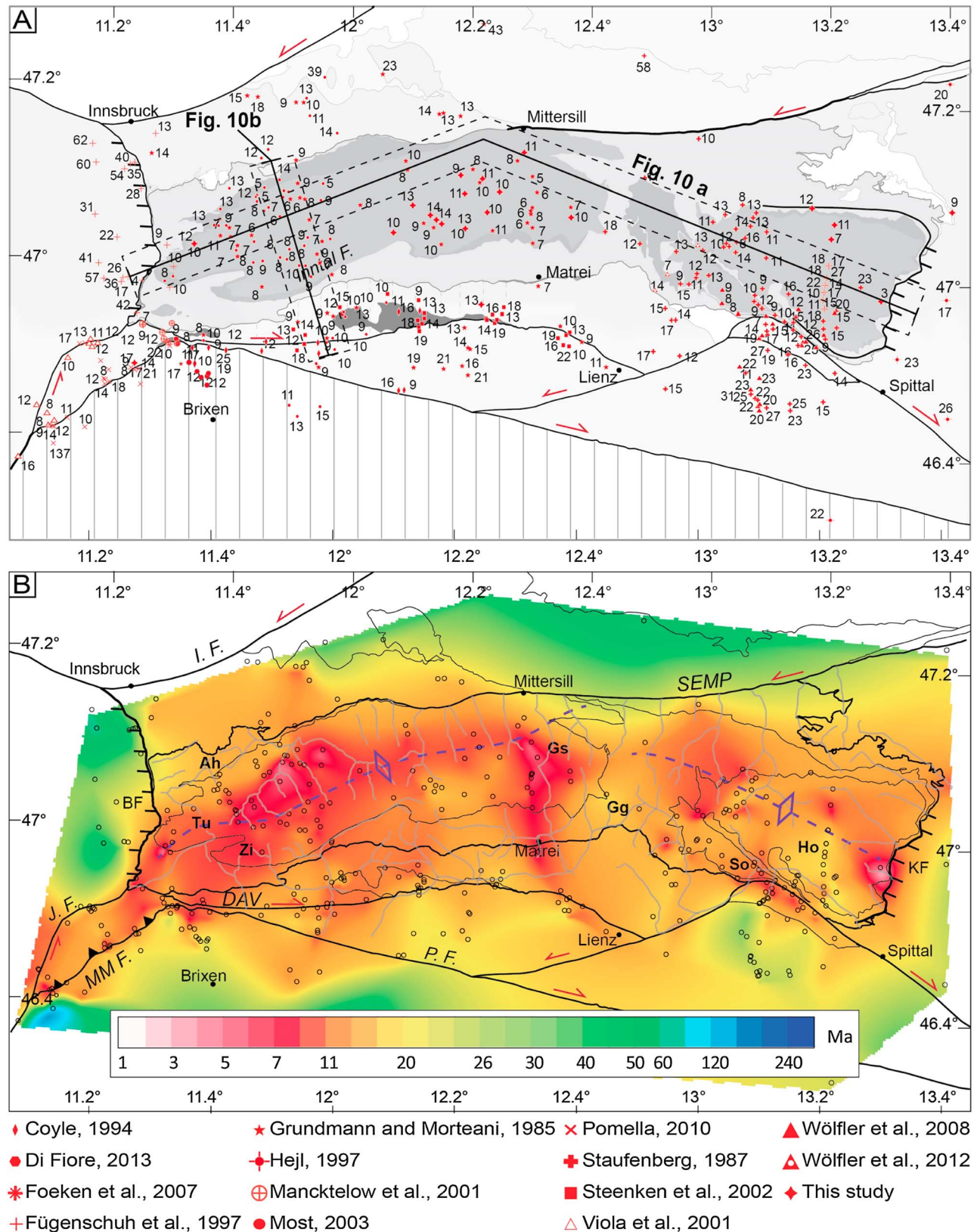
**Figure 9.** Distribution of compiled and new apatite fission track ages. (a) Dashed lines: spatial extent from which age data were projected to construct the cross sections of Figures 10a and 10b. Black lines: traces of cross sections of Figures 10a and 10b. (b) Interpolation of ages using the natural neighbor algorithm provided by Esri ArcMap 10™ GIS software. Legend as in Figure 8.
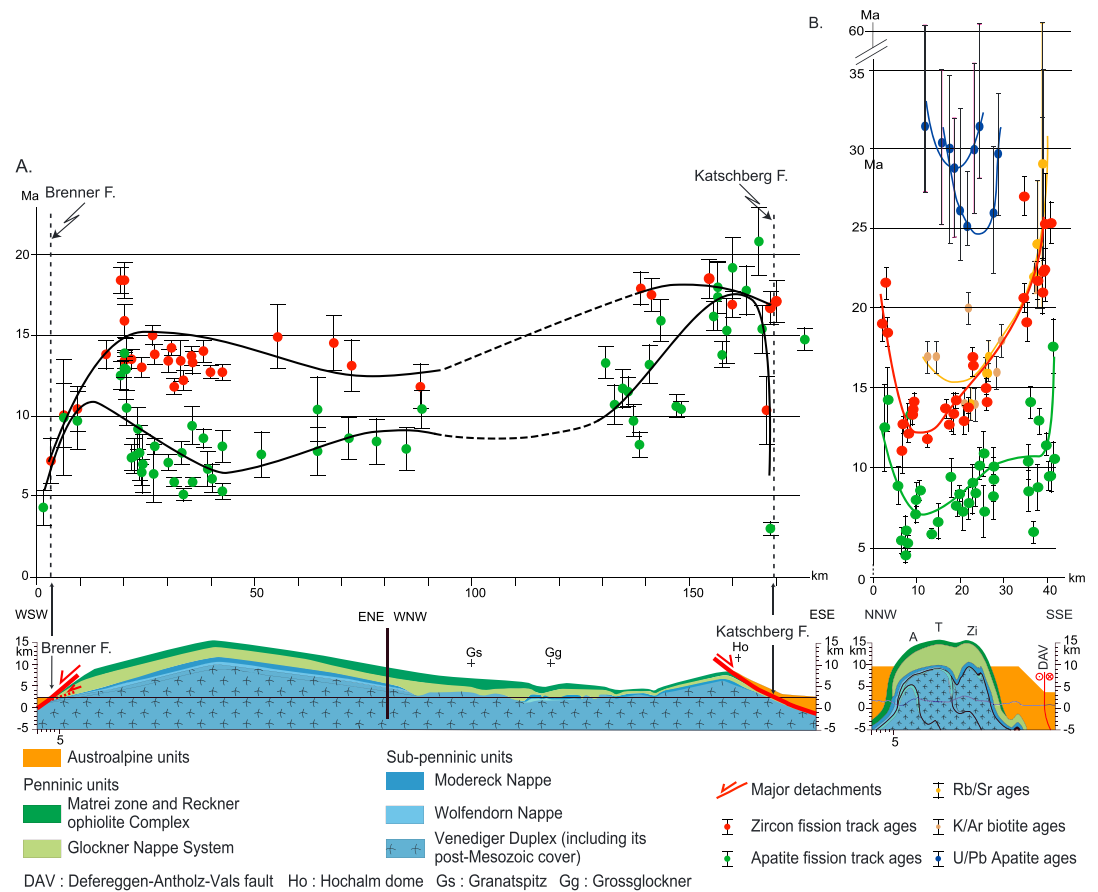
**Figure 10.** (a) Zircon and apatite fission track age distributions along a profile parallel to the main axial plane of the Tauern Dome. (b) Zircon and apatite fission track, Rb/Sr, K/Ar biotite, and U/Pb age distributions along a NNW-SSE profile through the western subdome (see Figures 8a and 9a for location). Ages were projected perpendicular to the profile from a distance of up to 5 km from each part of the profile trace. Cross sections are based on *Schmid et al.* [2013]. Rb/Sr and K/Ar biotite ages are from *Most* [2003], and U-Pb apatite ages are from *Schneider et al.* [2015].

As expected, apatite ages are systematically younger than zircon ages. In the west, the youngest ages (≤11 Ma) cover an elongate area that strikes ENE from the Meran-Mauls and Jaufen Faults to the Granatspitz area (Gs in Figure 9) in the central Tauern Window. This area coincides with the trace of the axial plane of the dome and is subparallel to the isograds (Figure 5). In the east, this area is less clearly defined but strikes WNW (Figure 9), also following the direction of the axial plane and of the isograds (Figure 5). As in the case of the zircons, apatite ages show a marked discontinuity across the Brenner Fault (from ~10 Ma in the footwall to more than 28 Ma in the hanging wall; Figure 9), whereas ages from the area between the Jaufen and Meran-Mauls Faults are similar to the ones of the western Tauern subdome [see also *Pomella*, 2010].

In contrast to zircon ages, apatites do not show a clear age jump across the DAV Fault (Figure 9) but range between 9 and 15 Ma both in the south and north of this structure (Figure 9), indicating that the DAV did not play an active role in the exhumation of the Tauern thermal dome (Figure 4) during the Late Miocene. Where present, apatite ages do not reveal an age jump across the northern boundary of the Tauern Window (Figure 9), suggesting that, from the Middle Miocene onward, both the Tauern Window and Austroalpine units further north were being exhumed at the same time [*Fügenschuh et al.*, 1997].

Sampling altitude may influence fission track ages, especially in areas affected by low exhumation rates, hence modifying the pattern of isoage lines on the local scale. In order to visualize the effect of sampling altitude, we extrapolated fission track ages to an arbitrarily chosen elevation of 1000 m based on the calculated slopes of age-altitude relationships (Figures S1 and S2 of supporting information). Such extrapolations show

that the main E-W elongate and concentric age pattern is slightly enhanced and that some of the N-S striking age contours largely disappear, especially for the apatite ages (Figures S1 and S2 of supporting information).

### 4.3. Profiles

In order to highlight the relationship between the major tectonic structures and possible age discontinuities and trends, zircon and apatite ages are plotted along two profiles, striking parallel (Figure 10a) and perpendicular (Figure 10b) to the main axial plane of the Tauern Dome. Rb/Sr ages, K/Ar biotite ages [*Most*, 2003], and U/Pb apatite ages [*Schneider et al.*, 2015] are also plotted along the profiles and perpendicular (Figure 12b) to the main axial plane of the upright fold. Due to the insufficient density of samples in the eastern subdome, especially zircon, we do not show a perpendicular section across the latter area.

Along the axial plane parallel section (Figure 10a), both zircon and apatite ages tend to become younger from east to west. However, within each subdome, ages increase toward the extensional fault bounding the dome but rapidly decrease in their immediate vicinity. The latter younging trend is only observed within a distance of ~20 km for the Brenner Fault and ~15 km for the Katschberg Fault (Figure 10a). The age versus distance diagram of the fold-perpendicular profile (Figure 10b) displays a bell shape for both the zircon and apatite ages, with younger ages located in the hinge of the dome (Figure 10b), resembling that of Figure 1b. These bell-shaped distributions recall those of cooling ages observed in other large-scale domes consisting of eroded anticlines [e.g., *Batt et al.*, 2001; *Willett and Brandon*, 2002].

The closure temperature for U-Pb on apatite is ≥450°C [*Chamberlain and Bowring*, 2000], and the closure temperature for the Rb/Sr and K/Ar systems is 300 ± 50°C [*Purdy and Jäger*, 1976]. These ages document the older exhumation history of the dome. Rb/Sr and K/Ar biotite [*Most*, 2003] and U-Pb apatite ages [*Schneider et al.*, 2015] also show a bell-shaped curve on the age versus distance diagram of Figure 10b. However, these bell shapes are less constrained than for the other method because of the small amount of data. The areas of maximum curvature of the U-Pb on apatite and Rb/Sr and K/Ar biotite curves are slightly shifted toward the south when compared to those of zircon and apatite fission track curves (Figure 10b). We suggest that this results from the formation of an antiformal stack of basement nappes that were progressively displaced northward. Therefore, the hinge of the bell for lower-*T* closure systems showing the younger cooling history is also displaced toward the north compared to the higher-*T* systems (Figure 10b).
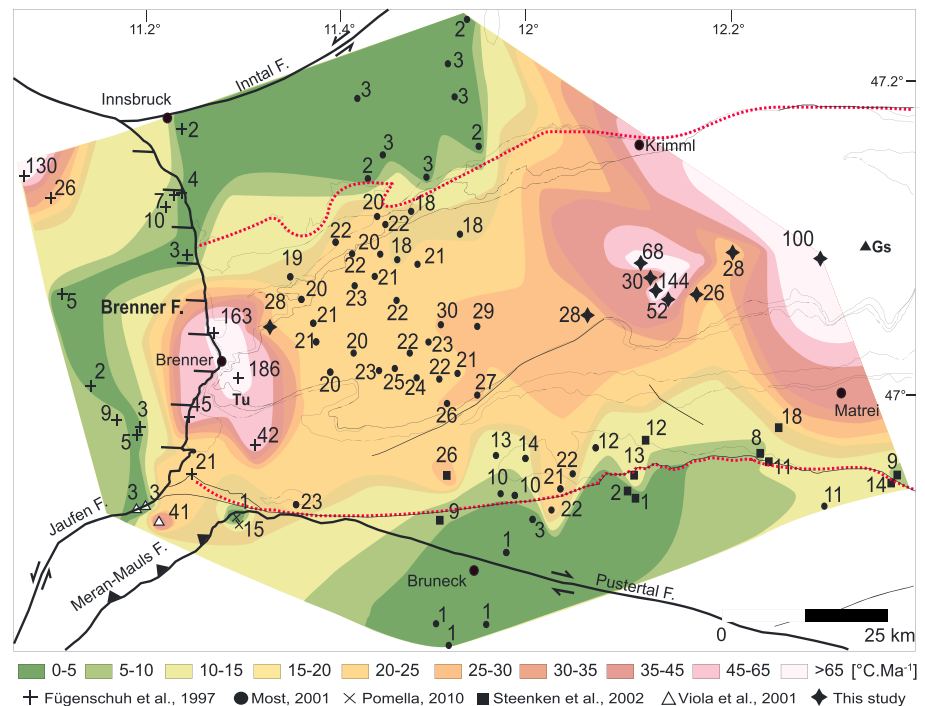
### 4.4. Cooling Rates

Based on paired samples providing both zircon and apatite ages, we determined cooling rates, for the temperature interval between the two closure temperatures. Precise values for closure temperatures are difficult to constrain because they depend on several parameters such as chemical composition, total accumulated radiation damages, and cooling rates [*Gleadow and Duddy*, 1982; *Kasuya and Naeser*, 1988]. In spite of these limitations and in order to visualize the spatial distribution of cooling rates, we used closure temperatures of 240 ± 60°C for zircon and 110 ± 20°C for F-rich apatites as currently estimated [*Yamada et al.*, 1995; *Green et al.*, 1986]. In the eastern subdome, only four samples were suitable; hence, a general pattern of cooling rates for this area cannot be assessed and we only show cooling rates of the western subdome and its surrounding Austroalpine units (Figure 11). Uncertainties on cooling rates are strongly affected by age errors. For the older samples surrounding the Tauern Dome, these errors result in uncertainties of ~10%, but for the younger samples, they attain 50%. In spite of these difficulties, Figure 11 shows a symmetric distribution of cooling rates, increasing toward the fold axial plane. The difference between cooling outside and inside the dome is larger than 1 order of magnitude.

### 4.5. Exhumation Rates

In order to calculate exhumation rates for the Tauern Window and surrounding areas, we inverted the thermochronometric data sets compiled above with the method described in *Herman and Brandon* [2015], which is a modified version of the method recently proposed by *Fox et al.* [2014, 2015]. This method exploits the information contained in both age elevation profiles and multithermochronometric system strategies (see *Fox et al.* [2014] for a detailed description of the inverse approach used here). The results of the inversion described above are illustrated by a series of time steps of 2 Ma, from 20 Ma to the present (Figure 12).

These data show that exhumation rates are heterogeneously distributed throughout the study area and through time. During a first phase of exhumation, between 20 and 10 Ma, the maximum rates were always

**Figure 11.** Cooling rates (in °C Ma$^{-1}$) based on samples providing both zircon and apatite ages. Dotted red lines show the limits of the Tauern thermal dome. In the south, it is based on the boundary between Cenozoic reset-unreset biotite Rb/Sr ages [*Borsi et al.*, 1973, 1978]; in the north, it is based on the limit between Cenozoic and Mesozoic zircon fission track ages [*Most*, 2003; *Fügenschuh et al.*, 1997].

located in the western subdome (always ≥0.5 mm a$^{-1}$, and locally attaining 0.9 mm a$^{-1}$) while exhumation of the eastern subdome remained relatively slow (≤0.4 mm a$^{-1}$). It is only from 8 Ma onward that exhumation rates became similar and slow (≤0.5 mm a$^{-1}$) throughout the Tauern Window (Figure 12). Finally, during the last 4 Ma, exhumation rates along the eastern and western margins of the dome became slightly faster than in its core. South of the Tauern Window, an area of nearly triangular shape is characterized by slow exhumation rates (≤0.25 mm a$^{-1}$) throughout the investigated time interval (Figure 12). This area was inferred to represent a microindenter during collision [*Scharf et al.*, 2013a].

## 5. Discussion

Progressive younging of ages toward the normal faults (Figure 10a) only takes place within an area of ~20 km distance from the Brenner Fault and 15 km from the Katschberg Fault, i.e., younging is only observed within the mylonitic belts of these normal fault systems (Figure 10a). Therefore, these age trends point to the younger activity of the faults, rather than to exhumation of the entire footwall due to normal faulting along the Brenner and Katschberg Faults. Large-scale, progressive younging would be expected if extensional denudation associated to exhumation paths parallel to the extensional direction (Figure 1a) had dominated unroofing of the Tauern Window.

In the western subdome, the elongate and concentric isoage contours of zircon (Figure 8b) and apatite (Figure 9b) are subparallel to both the axial plane of the Tauern Dome and the isograds of Barrovian metamorphism (Figure 5), suggesting that exhumation and cooling were mainly driven by folding and associated erosion. Late deformation of the isograds by upright folding or contemporaneous upright folding and bending of the isotherms would result in such a pattern.

The youngest ages along the dome-perpendicular cross section (Figure 10b) are located within the core of the western subdome (Figures 8, 9, and 10b), close to the northern limb of the dome (Figure 10b), probably reflecting an asymmetric construction by antiformal stacking of the nappes during northward thrusting [*Lammerer et al.*, 2008]. The minimum of the bell-shaped curve of the U-Pb on apatite data (Figure 10b)
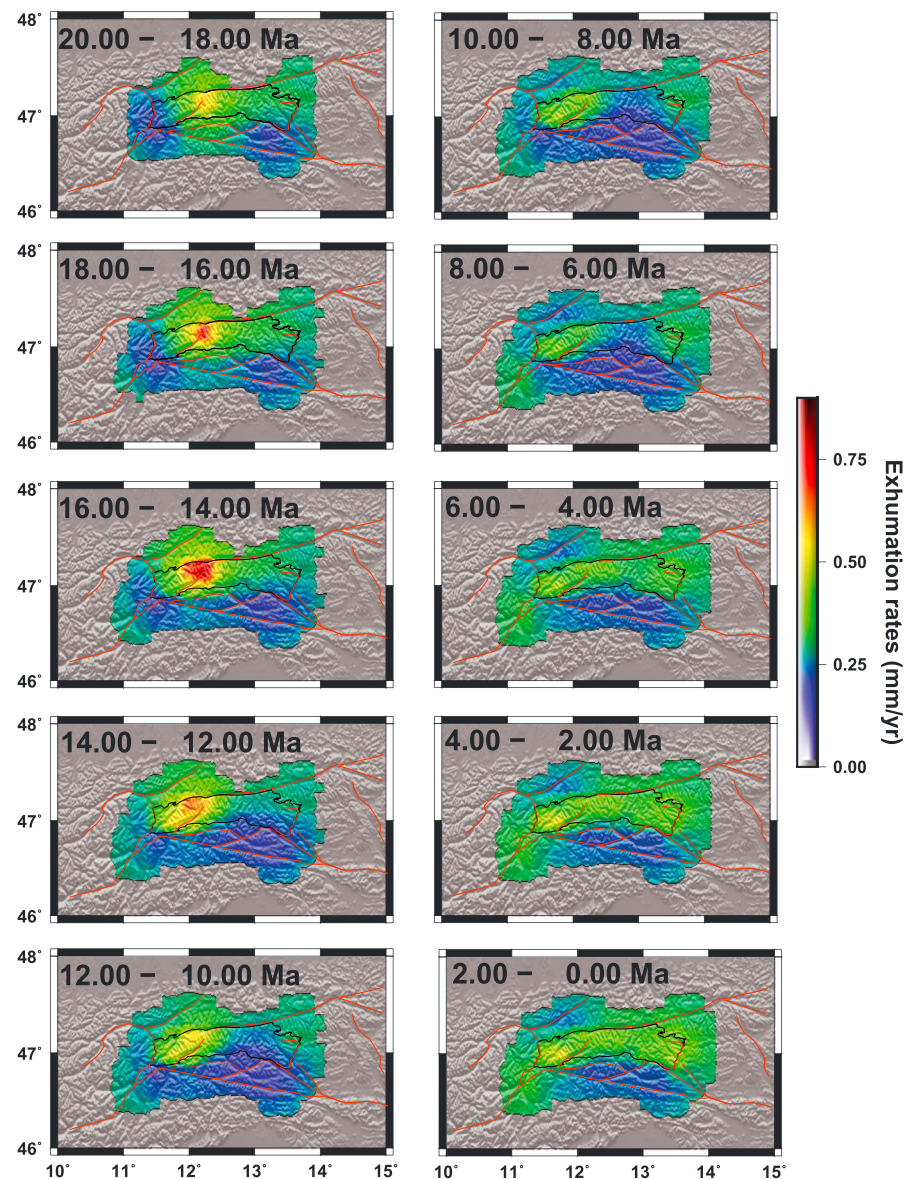
**Figure 12.** Exhumation rates calculated for intervals of 2 Ma over the past 20 Ma. Reduced variance corresponding to each exhumation interval is shown in Figure 3 of the supporting information. The models are obtained by inversion of apatite fission track ages [this study; *Dunkl et al.*, 2003; *Fügenschuh et al.*, 1997; *Mancktelow et al.*, 2001; *Most*, 2003; *Pomella*, 2010; *Steenken et al.*, 2002; *Stöckhert et al.*, 1999; *Viola et al.*, 2001; *Wölfler et al.*, 2008], zircon fission track ages [*Grundmann and Morteani*, 1985; *Staufenberg*, 1987; *Coyle*, 1994; *Hejl*, 1997; *Mancktelow et al.*, 2001; *Most*, 2003; *Viola et al.*, 2001; *Steenken et al.*, 2002; *Foeken et al.*, 2007; *Wölfer et al.*, 2008, 2012; *Pomella*, 2010; *Di Fiore*, 2013], and K/Ar ages [*Luth and Willingshofer*, 2008]. Black line represents the boundary of the Tauern Window. Red lines represent the main Cenozoic faults.

[*Schneider et al.*, 2015] is aligned with the minima of the curves of fission track ages, suggesting that cooling of all three thermochronological systems resulted from one and the same process. The age difference between apatite and zircon fission tracks in the hinge of the dome is smaller than in the limbs (Figure 10b), suggesting faster cooling in the core, as expected for exhumation during folding and erosion. Because the hinge of the antiform was exhumed from greater depths and at higher rates, it passed later than the limbs through the isotherms corresponding to zircon and apatite closure temperatures. This explains the younger ages of the hinge region (Figure 10b), as also illustrated by 2-D thermal models of shortening accommodated by folding and erosion [*Batt and Braun*; 1997; *Bertrand*, 2013]. Alternatively to folding and erosion, such age patterns may result from re-equilibration of the isotherms following their up-warping due to rapid uplift. In the first case, the bell-shaped curves of Figure 10 would form during doming of the Tauern Window, in the

latter case after doming. Considering the characteristic time of thermal equilibration of a structure having the size of the Tauern Dome, approximately 10 Ma is necessary. If this was the case, a large-scale shortening event, responsible for the up-warping of the isotherms in the area of the present-day Tauern Window, should have taken place before 40–35 Ma, i.e., 10 Ma before the ages of U-Pb on apatite (Figure 10b) [*Schneider et al.*, 2015]. This time interval is that of oceanic subduction in the Eastern Alps [*Schmid et al.*, 2013], which is not compatible with thickening and up-warping of isotherms in the continental, European plate.

According to the zircon and apatite ages (Figures 8 and 9) and the inferred exhumation rates (Figure 12), the area between the Jaufen Fault and the Dolomites Indenter was exhumed at similar rates and coevally with the Tauern Window. Structural investigations [*Schneider*, 2014] described the continuity of upright folds from the Tauern Window into this area, suggesting that all around the indenter corner exhumation was mainly controlled by folding and erosion accommodating shortening.

Exhumation rates calculated by inversion of thermochronometric data were mostly lower than 0.5 mm yr$^{-1}$ (Figure 12). If these rates are assumed to represent a maximum average over the past 15 Ma, they indicate 7.5 km of exhumation. Yet, in the western subdome, >20 km of exhumation was inferred based on geobarometric data [*Fügenschuh et al.*, 1997] and cross-section interpretations [*Schmid et al.*, 2013; *Rosenberg et al.*, 2015]. Since the onset of exhumation along the Brenner and Katschberg Faults is well constrained as Early Miocene (see *Schmid et al.* [2013] for discussion) and the total exhumation is on the order of 20 km [*Fügenschuh et al.*, 1997; *Schmid et al.*, 2013], pre-Miocene exhumation rates must have been higher than in the Miocene. This conclusion is in good agreement with the higher exhumation rates constrained for late Oligocene to Early Miocene time [*Von Blanckenburg et al.*, 1989; *Glodny et al.*, 2008; *Nagel et al.*, 2013; *Scharf et al.*, 2013b], which attained a maximum of 4 mm yr$^{-1}$ between 23 and 21 Ma [*Von Blanckenburg et al.*, 1989].

Based on the slightly older ages of the eastern subdome (Figure 10a), it was suggested that its unroofing initiated earlier than in the western subdome [*Dunkl et al.*, 2003; *Luth and Willingshofer*, 2008; *Favaro et al.*, 2016; *Scharf et al.*, 2016]. However, as shown by thermal models of folding designed to simulate the western subdome of the Tauern Window [*Bertrand*, 2013], material points exhumed in the hinge of the antiform, which stem from deeper crustal levels compared to those in the limbs, were uplifted at higher rates. The same is true for material points located in the hinge of an antiform of high amplitude (e.g., western subdome) compared to those located in the hinge of a fold of lower amplitude (e.g., eastern subdome) that underwent smaller amounts of shortening during the same time interval. Therefore, older ages in the eastern subdome may not represent its earlier exhumation [*Luth and Willingshofer*, 2008; *Scharf et al.*, 2013a, 2013b], but rather its slower exhumation compared to the western subdome, during one and the same, coeval folding event. Our interpretation relies on lateral changes of exhumation rates rather than on horizontal temperature variations that would otherwise attain as much as 300°C, as proposed by *Luth and Willingshofer* [2008]. Inversion of thermochronometric data confirms that between 20 and 10 Ma exhumation rates were significantly higher in the western subdome (Figure 12).

Coeval exhumation of the western and eastern subdomes, but at different rates, may be linked to the northward movement of the Dolomites Indenter [*Cornelius*, 1940], which is delimited by the straight, ESE striking Periadriatic Fault (Figures 2 and 13). An earlier interruption of exhumation in the eastern subdome is difficult to reconcile with the continuous and straight boundary of the Dolomites Indenter, which is inferred to cause shortening and folding in front of its margin. Moreover, a westward increase of shortening, leading to a westward increase of vertical thickening, hence uplift rates, is documented by the following structures: (1) the amplitude of upright folds in the western subdome is higher by ~10 km compared to the eastern subdome (Figures 3 and 13); (2) the width of the Austroalpine units involved in folding and shortening south of the Tauern Window decreases progressively westward (Figures 2 and 13) and this change of width is associated with a westward tightening of upright folds [*Wagner et al.*, 2006], hence, to increased shortening; (3) the Oligocene Periadriatic Fault was straight and E-W striking before being sinistrally offset by the Giudicarie Fault (Figure 2) during Oligo-Miocene times, which accommodated the northward movement of the Dolomites Indenter [e.g., *Laubscher*, 1971; *Schmid et al.*, 1996; *Schmid and Kissling*, 2000; *Pomella*, 2010]. The change from its E-W strike to the present-day ESE strike (Figure 2) reflects a clockwise rotation of the Dolomites Indenter (Figure 13), leading to progressively larger displacements toward the indenter corner.

Taken together, the distribution of exhumation rates reflects a two-stage process. A first Early to Middle Miocene stage, mainly driven by folding and erosion, coincided with the amplification of upright folds and
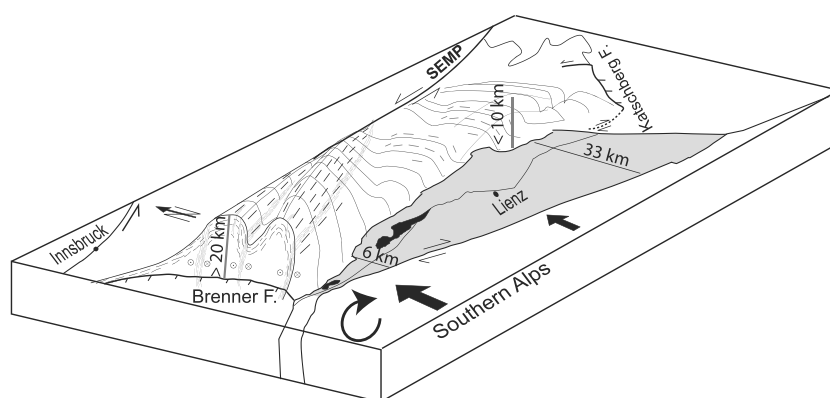
**Figure 13.** Simplified sketch of Tauern Window and surrounding areas illustrating a clockwise rotation of the Dolomites Indenter, causing a westward increase of shortening and uplift rates in the Tauern Window. A westward reduction of the width of the Austroalpine south of the Tauern Window (gray area) from 33 to 6 km and a westward increase of fold amplitude (10 to 20 km) document this along-strike structural change.

high exhumation rates in the western subdome (Figure 12). Normal faulting along the Brenner and Katschberg Faults decoupled the folding footwalls from their largely unfolded hanging walls. The young ages in the vicinity of the Brenner Fault (Figures 8, 9, and 10a), the late, modest increase of exhumation rates in the footwalls of the Katschberg and Brenner Faults (Figure 12), and the absence of brittle structures pointing to N-S shortening [*Bertrand et al.*, 2015] suggest the existence of a second, minor stage of exhumation of Pliocene age that was mainly driven by extensional unroofing along the Brenner and Katschberg Faults.

## 6. Conclusions

Compilations of previous and new zircon and apatite fission track ages provide a complete picture of the distribution of cooling ages over the Tauern Window and surrounding areas. In particular, the new zircon ages in the central Tauern Window allowed us to trace for the first time isoage contour maps, linking the western and eastern subdomes.

The spatial coincidence between the antiformal structure and the bell shape of fission track ages on age/distance diagrams and the absence of large-scale younging of ages in the footwall, toward the major normal faults at the dome margins, suggest that upright folding and erosion were the major processes controlling exhumation of the Tauern Dome in the time span given by zircon and apatite fission track ages, i.e., during most of the Miocene. The young zircon and apatite ages found in the mylonitic zones of the Katschberg and Brenner Faults and the modest increased exhumation rates in the vicinity of these faults during Pliocene times (Figure 12) attest to a young activity of the latter structures that was possibly dominated by extensional unroofing during this latest phase of exhumation.

The concentric isoage contour lines, subparallel and almost symmetrically distributed about the hinge of the western subdome, correspond to the age distributions expected from upright antiformal folding. The entire Miocene exhumation history of the Tauern Window is marked by faster exhumation of the western subdome compared to the eastern subdome. Only after 6 Ma did the exhumation rates become similar, and slow, in both subdomes. Exhumation of the lower-amplitude, flat-lying hinge area of the eastern dome occurred at the same time but at lower rates. The spatial, more homogeneous distribution of cooling ages and of exhumation rates in the eastern subdome compared to the western subdome is consistent with the plateau-type fold geometry of the former and the high amplitude of the latter.

In spite of older ages of samples from the eastern subdome, exhumation rates show that exhumation did not start nor terminate earlier in the eastern compared to western Tauern Window. Inversion of thermochronometric ages shows that the lower exhumation rates in the eastern subdome adequately explain the age difference. Lower exhumation rates are inferred to result from lower uplift rates during folding, because the wavelength of the eastern subdome is larger and its amplitude is lower compared to the western subdome. This interpretation is consistent with the idea of a single shortening and folding event in the

Tauern Window, accommodating one and the same indentation process. Larger displacements of the indenter in the west resulted in higher amounts of shortening, hence higher uplift and exhumation rates and younger cooling ages in the western subdome. These relationships suggest a clockwise rotation of the Dolomites Indenter and a control of upright folding on Miocene exhumation in the Tauern Window.

# References

Axen, G. J., J. M. Bartley, and J. Selverstone (1995), Structural expression of a rolling hinge in the footwall of the Brenner Line normal fault, Eastern Alps, *Tectonics*, *14*, 1380–1392, doi:10.1029/95TC02406.

Batt, G. E., and J. Braun (1997), On the thermomechanical evolution of compressional orogens, *Geophys. J. Int.*, *128*, 364–382, doi:10.1111/j.1365-246X.1997.tb01561.x.

Batt, G. E., M. T. Brandon, K. A. Farley, and M. Roden-Tice (2001), Tectonic synthesis of the Olympic Mountains segment of the Cascadia wedge, using two-dimensional thermal and kinematic modelling of thermochronological ages, *J. Geophys. Res.*, *106*, 731–746, doi:10.1029/2001JB000288.

Behrmann, J. H. (1988), Crustal-scale extension in a convergent orogen: The Sterzing-Steinach mylonite zone in the Eastern Alps, *Geodynam. Acta*, *2*, 63–73, doi:10.1080/09853111.1988.11105157.

Berner, H., H. Hamberg, and O. Stephansson (1972), Diapirism in theory and experiment, *Tectonophysics*, *15*, 197–218.

Bertrand, A. (2013), Exhuming the core of collisional orogen, the Tauern Window (Eastern Alps). A geochronological, modelling and structural study, PhD thesis, Freie Universität, Berlin.

Bertrand, A., C. L. Rosenberg, and S. Garcia (2015), Fault slip analysis and late exhumation of the Tauern Window, Eastern Alps, *Tectonophysics*, *649*, 1–17, doi:10.1016/j.tecto.2015.01.002.

Borsi, S., A. Del Moro, and F. Sassi (1973), Metamorphic evolution of the Austridic rocks to the south of the Tauern Window (Eastern Alps): Radiometric and geopetrological data, *Mem. Soc. Geol. It.*, *12*, 549–571.

Borsi, S., A. Del Moza, F. Sassi, A. Zanferrari, and G. Zirpoli (1978), New geopetrologic and radiometric data on the alpine history of the Austridic continental margin South of the Tauern window (Eastern Alps), *Mem. Istituto della Regia Univ. di Padova*, *32*, 1–17.

Bousquet, R., R. Oberhänsli, B. Goffé, M. Wiederkehr, F. Koller, S. M. Schmid, R. Schuster, M. Engi, A. Berger, and G. Martinotti (2008), Metamorphism of metasediments in the scale of an orogen: A key to the Tertiary geodynamic evolution of the Alps, in *Tectonic Aspects of the Alps-Dinarides-Carpathians*, Geol. Soc. Lond. Spec. Publ., vol. 298, edited by S. Siegesmund, B. Fügenschuh, and N. Froitzheim, pp. 393–411.

Brichau, S., U. Ring, R. A. Ketcham, A. Carter, D. Stockli, and M. Brunel (2006), Constraining the long-term evolution of the slip rate for a major extensional fault system in the central Aegean, Greece, using thermochronology, *Earth Planet. Sci. Lett.*, *241*, 293–306.

Brun, J. P., and J. Van Den Driessche (1994), Extensional gneiss domes and detachment fault-systems: Structure and kinematics, *Bull. Soc. Geol. Fr.*, *165*, 519–530.

Burg, J. P., B. J. P. Kaus, and Y. Y. Podladchikov (2004), Dome structures in collision orogens: Mechanical investigations of the gravity/compression interplay, in *Gneiss Domes in Orogeny: The Geological Society of America*, Spec. Pap., vol. 380, edited by D. Whitney, C. Teyssier, and S. Siddoway, pp. 47–66.

Chamberlain, K. R., and S. A. Bowring (2000), Apatite-feldspar U-Pb thermochronometer: A reliable, mid-range (~450 °C), diffusion-controlled system, *Chem. Geol.*, *172*, 173–200.

Christensen, J. N., J. Selverstone, J. L. Rosenfeld, and D. J. DePaolo (1994), Correlation by Rb-Sr geochronology of garnet growth histories from different structural levels within the Tauern Window, Eastern Alps, *Contrib. Mineral. Petrol.*, *118*, 1–12, doi:10.1007/BF00310607.

Cliff, R. A., F. Oberli, M. Meier, G. T. R. Droop, and M. Kelly (2015), Syn-metamorphic folding in the Tauern Window, Austria dated by Th-Pb ages from individual allanite porphyroblasts, *J. Metamorph. Geol.*, *33*, 427–435, doi:10.1111/jmg.12127.

Coney, P. J., and T. A. Harms (1984), Metamorphic core complexes: Cenozoic extensional relics of Mesozoic compression, *Geology*, *12*, 550–554.

Cornelius, H. P. (1940), Zur Auffassung der Ostalpen im Sinne der Deckenlehre, *Zeitsch. Deutsch. Geol. Ges.*, *92*, 271–312.

Coyle, D. A. (1994), The application of apatite fission-track analysis to problem in tectonics, PhD thesis, La Trobe Univ. Bundoora, Victoria, Australia.

Crittenden, M. D., P. J. Coney, and G. H. Davis (Eds.) (1980), *Cordilleran Metamorphic Core Complexes*, Geol. Soc. Am. Mem., vol. 153, pp. 490.

Crowley, K. D., M. Cameron, and R. L. Schaefer (1991), Experimental studies of annealing of etched fission-tracks in fluorapatite, *Geochim. Cosmochim. Acta*, *55*, 11,449–11,465, doi:10.1016/0016-7037(91)90320-5.

Davis, G. H., and P. J. Coney (1979), Geologic development of the Cordilleran metamorphic core complexes, *Geology*, *7*(3), 120–124, doi:10.1130/0091-7613(1979).

Decker, K., and H. Peresson (1996), Tertiary kinematics in the Alpine-Carpathian-Pannonian system: Links between thrusting, transform faulting and crustal extensions, in *Oil and Gas in Alpidic Thrustbelts and Basins of Central and Eastern Europe*, EAGE, Spec. Publ., vol. 5, edited by G. Wessely and W. Liebl, pp. 69–77.

Di Fiore, G. (2013), Evoluzione Morfotettonica delle aree alpine "Sempione" e "Brennero" attraverso studi termocronologici di bassa temperatura, PhD thesis, Università di Bologna.

Donelick, R. A. (1993), Apatite etching characteristics versus chemical composition, *Nucl. Tracks Radiat. Meas.*, *21*, 604.

Donelick, R. A., R. Ketcham, and W. D. Carlson (1999), Variability of apatite fission-track annealing kinetics II: Crystallographic orientation effects, *Am. Mineral.*, *84*, 1224–1234.

Donelik, R. A., P. B. O'Sullivan, and R. Ketcham (2005), Apatite fission-track analysis, *Rev. Mineral. Geochem.*, *58*, 49–94, doi:10.2138/rmg.2005.58.3.

Dunkl, I. (2002), TRAKKEY: A Windows program for calculating and graphical presentation of fission-track data, *Comput. Geosci.*, *28*, 3–12.

Dunkl, I., W. Frisch, and G. Grundmann (2003), Zircon fission-track thermochronology of the south-eastern part of the TW and the adjacent Austroalpine margin, Eastern Alps, *Eclogae Geol. Helv.*, *96*, 209–217, doi:10.1007/s00015-003-1092-3.

Eskola, P. E. (1949), The problem of mantle gneiss domes, *Q. J. Geol. Soc. London*, *104*, 253–283.

Favaro, S., R. Schuster, M. R. Handy, A. Scharf, and G. Pestal (2016), Transition from orogen-perpendicular to orogen-parallel exhumation and cooling during crustal indentation—Key constraints from 147Sm/144Nd and 87Rb/86Sr geochronology (Tauern Window, Alps).

Foeken, J. P. T., C. Persano, F. M. Stuart, and M. ter Voorde (2007), Role of topography in isotherm perturbation: Apatite (U-Th)/He and fission-track results from the Malta tunnel, Tauern Window, Austria, *Tectonics*, *26*, TC3006, doi:10.1029/2006TC002049.

Foster, D. A., C. Schafer, M. C. Fanning, and D. W. Hyndmann (2001), Relationships between crustal partial melting, plutonism, orogeny, and exhumation: Idaho-Bitterroot batholith, *Tectonophysics*, *342*, 313–350, doi:10.1016/S0040-1951(01)00169-X.

Foster, D. A., W. C. Grice, and T. J. Kalakay (2010), Extension of the Anaconda metamorphic core complex: [40]Ar/[39]Ar thermochronology and implications for Eocene tectonics of the northern Rocky Mountains and the Boulder batholith, *Lithosphere*, *2*, 232–246.

Fox, M., F. Herman, S. D. Willett, and D. A. May (2014), A linear inversion method to infer exhumation rates in space and time from thermochronometric data, *Earth Surf. Dyn.*, *2*, 47–65, doi:10.5194/esurf-2-47-2014.

Fox, M., F. Herman, E. Kissling, and S. D. Willett (2015), Rapid exhumation in the Western Alps driven by slab detachment and glacial erosion, *GSA*, doi:10.1130/G36411.1.

Frank, W., M. Kralik, S. Scharbert, and M. Thöni (1987), Geochronological data from the Eastern Alps, in *Geodynamics of the Eastern Alps*, edited by H. W. Flügel and P. Faulp, pp. 272–281, Deuticke, Wien.

Frisch, W., A. Kuhlemann, I. Dunkl, and A. Brügel (1998), Palinspastic reconstruction and topographic evolution of the Eastern Alps during late Tertiary tectonic extrusion, *Tectonophysics*, *297*, 1–15, doi:10.1016/S0040-1951(98)00160-7.

Frisch, W., I. Dunkl, and J. Kuhlemann (2000), Post-collisional orogen-parallel large-scale extension in the Eastern Alps, *Tectonophysics*, *327*, 239–265, doi:10.1016/S0040-1951(00)00204-3.

Fügenschuh, B., D. Seward, and N. S. Mancktelow (1997), Exhumation in a convergent orogen: The western Tauern Window, *Terra Nova*, *9*, 213–217, doi:10.1111/j.1365-3121.1997.tb00015.x.

Fügenschuh, B., N. S. Mancktelow, and S. M. Schmid (2012), Comment on Rosenberg and Garcia: Estimating displacement along the Brenner Fault and orogen-parallel extension in the Eastern Alps, Int J Earth Sci (Geol Rundsch) (2011) 100:1129–1145, *Int. J. Earth. Sci.*, *101*, 1451–1455, doi:10.1007/s00531-011-0725-4.

Garver, J., P. W. Reiners, L. J. Walker, J. M. Ramage, and S. E. Perry (2005), Implication of timing of Andean uplift from thermal resetting of radiation-damaged zircon in the Cordillera Huayhuash, Northern Peru, *J. Geol.*, *1113*, 117–138, doi:10.1086/427664.

Genser, J., and F. Neubauer (1989), Low angle normal faults at the eastern margin of the Tauern Window (Eastern Alps), *Mitt. Österr. Geol. Gs.*, *81*, 233–243.

Genser, J., J. D. van Wees, S. Cloetingh, and F. Neubauer (1996), Eastern Alpine tectono-metamorphic evolution: Constraints from two-dimensional *P-T-t* modeling, *Tectonics*, *15*(2), 584–604, doi:10.1029/95TC03289.

Gleadow, A. J. W. (1981), Fission-track dating methods: What are the real alternatives?, *Nucl. Tracks*, *5*, 3–14.

Gleadow, A. J. W., and I. R. Duddy (1982), A natural long-term annealing experiment for apatite, *Nucl. Tracks Radiat. Exp.*, *5*, 169–174.

Glodny, J., U. Ring, and A. Kühn (2008), Coeval high-pressure metamorphism, thrusting, strike-slip, and extensional shearing in the Tauern Window, Eastern Alps, *Tectonics*, *27*, TC4004, doi:10.1029/2007TC002193.

Green, P. F., I. R. Duddy, A. J. W. Gleadow, P. R. Tingate, and G. M. Laslett (1985), Fission-track annealing in apatite: Track length measurements and the form of the Arrhenius plot, *Nucl. Tracks*, *10*, 323–328.

Green, P. F., I. R. Duddy, A. J. W. Gleadow, P. R. Tingate, and G. M. Laslett (1986), Thermal annealing of fission-tracks in apatite. 1. A qualitative description, *Chem. Geol.*, *59*, 237–253.

Green, P. F., I. R. Duddy, G. M. Laslett, K. A. Hegarty, A. J. W. Gleadow, and J. F. Lovering (1989), Thermal annealing of fission-tracks in apatite. 4. Quantitative modeling techniques and extension to geological timescales, *Chem. Geol.*, *79*, 155–182.

Grundmann, G., and G. Morteani (1985), The young uplift and thermal history of the central Eastern Alps (Austria/Italy), evidence from apatite fission-track ages, *Jahrbuch der Geol. Bundesanst.*, *128*, 197–216.

Handy, M., and R. Oberhänsli (2004), Age of the metamorphic structure of the Alps—Tectonic interpretation and outstanding problems, in *Explanatory Notes to the Map: Metamorphic Structure of the Alps*, *Mitteilungen der Österreichischen Mineral. Gesellschaft*, vol. 149, edited by R. Oberhänsli, pp. 97–121.

Handy, M. R., S. M. Schmid, R. Bousquet, E. Kissling, and D. Bernoulli (2010), Reconciling plate-tectonic reconstructions of Alpine Tethys with the geological-geophysical record of spreading and subduction in the Alps, *Earth Sci. Rev.*, *102*(3–4), 121–158, doi:10.1016/j.earscirev.2010.06.002.

Hejl, E. (1997), 'Cold spots' during the Cenozoic evolution of the Eastern Alps: Thermochronological interpretation of apatite fission-track data, *Tectonophysics*, *272*, 159–173, doi:10.1016/S0040-1951(96)00256-9.

Herman, F., and M. Brandon (2015), Mid-latitude glacial erosion hotspot related to equatorial shifts in southern Westerlies, *Geology*, doi:10.1130/G37008.1.

Hoernes, S., and H. Friedrichsen (1974), Oxygen isotope studies of metamorphic rocks of the Western Hohe Tauern Area (Austria), *Schweiz. Mineral. Petrogr. Mitt.*, *54*, 769–788.

Hoinkes, G., F. Koller, G. Rantitsch, E. Dachs, V. Hock, F. Neubauer, and R. Schuster (1999), Alpine metamorphism of the Eastern Alps, *Schweiz. Mineral. Petrogr. Mitt.*, *79*, 155–181.

Hurford, A. J., and P. F. Green (1983), The zeta age calibration of fission-track dating, *Chem. Geol.*, *41*, 285–317.

Inger, S., and R. A. Cliff (1994), Timing of metamorphism in the Tauern Window, Eastern Alps: Rb-Sr ages and fabric formation, *J. Met. Geol.*, *12*, 695–707, doi:10.1111/j.1525-1314.1994.tb00052.x.

Jolivet, L., V. Famin, C. Mehl, T. Parra, C. Aubourg, R. Hébert, and P. Philippot (2004), Strain localization during crustal-scale boudinage to form extensional metamorphic domes in the Aegean Sea, in *Gneiss Domes in Orogeny*, vol. 380, edited by D. L. Whitney, C. Teyssier and C. S. Siddoway, pp. 185–210, *Geol. Soc. Am. Spec. Pap.*, Boulder, Colo., doi:10.1130/0-8137-2380-9.185.

Kasuya, M., and C. W. Naeser (1988), The effect of α-damage on fission-track annealing in zircon, *Int. J. Radiat. Appl. Instrum. Part D*, *14*, 477–480, doi:10.1016/1359-0189(88)90008-8.

Kleinschrodt, R. (1987), *Quarzkorngefügeanalyse im Altkristallin südlich des westlichen Tauernfensters (Südtirol/Italien)*, vol. 114, pp. 1–82, Erlanger Geol. Abh., Erlangen, Germany.

Kuhlemann, J., W. Frisch, I. Dunkl, and B. Székely (2001), Quantifying tectonic versus erosive denudation: The Miocene core complexes of the Alps, *Tectonophysics*, *330*, 1–23, doi:10.1016/S0040-1951(00)00209-2.

Lammerer, B. (1988), Thrust-regime and transpression regime tectonics in the Tauern Window (Eastern Alps), *Geol. Rundsch.*, *77*, 143–156, doi:10.1007/BF01848681.

Lammerer, B., and M. Weger (1998), Footwall uplift in an orogenic wedge: The Tauern Window in the Eastern Alps of Europe, *Tectonophysics*, *285*, 213–230.

Lammerer, B., H. Gebrande, E. Lüschen, and P. Vesela (2008), A crustal-scale cross section through the Tauern Window (Eastern Alps) from geophysical and geological data, in *Tectonic Aspects of the Alpsine-Carpathian-Dinaride System*, edited by S. Siegesmund, B. Fügenschuh, and N. Froitzheim, *Geol. Soc. Spec. Publ.*, pp. 219–229.

Laubscher, H. P. (1971), Das Alpen-Dinariden-Problem und die Palinspastik der südlichen Tethys, *Int. J. Earth Sci.*, *40*, 813–833.

Laubscher, H. P. (1988), Material balance in Alpine orogeny, *Geol. Soc. Am. Bull.*, *100*, 1313–1328, doi:10.1130/0016-7606.

Linzer, H. G., L. Ratschbacher, and W. Frisch (1995), Transpressional collision structures in the upper crust: The fold-thrust belt of the Northern Calcareous Alps, *Tectonophysics*, *242*, 41–61.

Linzer, H. G., K. Decker, H. Peresson, R. Dell'Mour, and W. Frisch (2002), Balancing orogenic float of the Eastern Alps, *Tectonophysics*, *354*, 211–237, doi:10.1016/S0040-1951(02)00337-2.

Luth, S. W., and E. Willingshofer (2008), Mapping of the post-collisional cooling history of the Eastern Alps, *Swiss J. Geosci.*, *101*(1), 201–223, doi:10.1007/s00015-008-1294-9.

Mancktelow, N. S., and T. L. Pavlis (1994), Fold-fault relationships in low-angle detachment systems, *Tectonics*, *13*, 668–685, doi:10.1029/93TC03489.

Mancktelow, N. S., D. F. Stöckli, B. Grollimund, W. Müller, B. Fügenschuh, G. Viola, D. Seward, and I. M. Villa (2001), The DAV and Periadriatic fault systems in the Eastern Alps south of the Tauern Window, *Int. J. Earth Sci.*, *90*, 593–622, doi:10.1007/s005310000190.

Most, P. (2003), Late Alpine cooling histories of tectonic blocks along the central part of the Transalp-Traverse (Inntal-Gadertal): Constraints from geochronology, PhD thesis, p. 97, Univ. of Tübingen.

Müller, W., G. Prosser, N. S. Mancktelow, I. M. Villa, S. P. Kelley, G. Viola, and F. Oberli (2001), geochronological constraints on the evolution of the Periadriatic fault system (Alps), *Intern. J. Earth Sci.*, *90*(3), 623–653.

Nagel, T. J., D. Herwartz, S. Rexroth, C. Münker, N. Froitzheim, and W. Kurz (2013), Lu-Hf dating, petrography, and tectonic implications of the youngest Alpine eclogites (Tauern Window, Austria), *Lithos*, *170–171*, 179–190, doi:10.1016/j.lithos.2013.02.008.

Neubauer, F., J. Genser, W. Kurz, and X. Wang (1999), Exhumation of the Tauern Window, Eastern Alps, *Phys. Chem. Earth, Ser. A*, *24*, 675–680, doi:10.1016/S1464-1895(99)00098-8.

Neubauer, F., J. Genser, and R. Handler (2000), The Eastern Alps: Result of a two-stage collision process, *Mitt. Österr. Geol. Ges.*, *92*, 117–134.

Nollau, G. (1969), Kleintektonische Strukturen am Südrand des Tauernfensters und ihre Einbeziehung in großtektonische Konzepte, *Geol. Rundsch.*, *58*, 755–788.

O'Sullivan, P. B., and R. R. Parrish (1995), The importance of apatite composition and single-grain ages when interpreting fission-track data from plutonic rocks: A case study from the Coast Ranges, British Columbia, *Earth Planet. Sci. Lett.*, *132*, 213–224, doi:10.1016/0012-821X(95)00058-K.

Oberhänsli, R., et al. (2004), Metamorphic structure of the Alps. Scale 1:1,000,000, Commission for the Geological Map of the World, Paris.

Peresson, H., and K. Decker (1997), The Tertiary dynamics of the northern Eastern Alps (Austria): Changing palaeostress in a collisional plate boundary, *Tectonophysics*, *272*, 125–157.

Pomella, H. (2010), The Cenozoic evolution of the Giudicarie fault system (Eastern/Southern Alps, northern Italy). A geochronological, structural and paleomagnetic study, PhD thesis, Institute of Geology and Paleontology, Univ. of Innsbruck.

Purdy, J. W., and E. Jäger (1976), *K-Ar Ages on Rock Forming Minerals From the Central Alps*, vol. 30, pp. 1–31, Mem. Ist. Geol. Min. Univ, Padova.

Ramsay, J. G. (1967), *Folding and Fracturing of Rocks*, pp. 568, McGraw-Hill, New York.

Ratschbacher, L., O. Merle, P. Davy, and P. Cobbold (1991), Lateral extrusion in the Eastern Alps, Part. 1: Boundary conditions and experiments scaled for gravity, *Tectonics*, *10*, 245–256, doi:10.1029/90TC02622.

Reddy, S. M., R. A. Cliff, and R. East (1993), Thermal history of the Sonnblick Dome, south-east Tauern Window, Austria: Implications for heterogeneous uplift within the Pennine basement, *Geol. Rdsch.*, *82*, 667–675, doi:10.1007/BF00191494.

Rosenberg, C. L., and A. Berger (2009), On the causes and modes of lateral growth of the Alps, *Tectonics*, *28*, TC6001, doi:10.1029/2008TC002442.

Rosenberg, C. L., and S. Garcia (2011), Estimating displacement along the Brenner fault and orogen parallel extension in the Eastern Alps, *Int. J. Earth. Sci.*, *100*, 1129–1145, doi:10.1007/s00531-011-0645-3.

Rosenberg, C. L., and S. Garcia (2012), Reply to the comment of Fügenschuh et al. on the paper "Estimating displacement along the Brenner Fault and orogen-parallel extension in the Eastern Alps" by Rosenberg and Garcia, Int. J. Earth Sci. (Geol Rundsch) 100:1129–1145, *Int. J. Earth. Sci.*, *101*, 1457–1464, doi:10.1007/s00531-011-0726-3.

Rosenberg, C. L., and S. Schneider (2008), The western termination of the SEMP fault (Eastern Alps) and its bearing on the exhumation of the TW, in *Tectonics Aspects of the Alpine-Dinaride-Carpathian System*, edited by S. Siegesmund, B. Fügenschuh, N. Froitzheim, *Geol. Soc. London*, 298, 197-218, doi:10.1144/SP298.10.

Rosenberg, C. L., J.-P. Brun, and D. Gapais (2004), Indentation model of the Eastern Alps and the origin of the Tauern Window, *Geology*, *32*, 997–1000, doi:10.1130/G20793.1.

Rosenberg, C. L., J.-P. Brun, F. Cagnard, and D. Gapais (2007), Oblique indentation in the Eastern Alps: Insights from laboratory experiments, *Tectonics*, *26*, TC2003, doi:10.1029/2006TC001960.

Rosenberg, C. L., A. Berger, N. Bellahsen, and R. Bousquet (2015), Relating orogen width to shortening, erosion, and exhumation during Alpine collision, *Tectonics*, *34*, 1306–1328, doi:10.1002/2014TC003736.

Scharf, A., M. R. Handy, S. Favaro, S. M. Schmid, and A. Bertrand (2013a), Modes of orogen-parallel stretching and extensional exhumation in response to microplate indentation and roll-back subduction (Tauern Window, Eastern Alps), *Int. J. Earth Sci.*, doi:10.1007/s00531-013-0894-4.

Scharf, A., M. R. Handy, M. A. Ziemann, and S. M. Schmid (2013b), Peak-temperature patterns of polyphase metamorphism resulting from accretion, subduction and collision (eastern Tauern Window, European Alps)—A study with Raman microspectroscopy on carbonaceous material (RSCM), *J. Metamorph. Geol.*, *31*, 863–880, doi:10.1111/jmg.12048.

Scharf, A., M. R. Handy, S. M. Schmid, S. Favaro, M. Sudo, R. Schuster, and K. Hammerschmidt (2016), Grain-size effects on the closure temperature of white mica in a crustal-scale extensional shear zone—Implications of in-situ 40Ar/39Ar laser-ablation of white mica for dating shearing and cooling (Tauern Window, Eastern Alps), *Tectonophysics*, *674*, 210–226, doi:10.1016/j.tecto.2016.02.014.

Schmid, S. M., and E. Kissling (2000), The arc of the western Alps in the light of geophysical data on deep crustal structure, *Tectonics*, *19*, 62–85, doi:10.1029/1999TC900057.

Schmid, S. M., O. Pfiffner, N. Froitzheim, G. Schönborn, and E. Kissling (1996), Geophysical-geological transect and tectonic evolution of the Swiss-Italian Alps, *Tectonics*, *15*, 1036–1064, doi:10.1029/96TC00433.

Schmid, S. M., A. Scharf, M. R. Handy, and C. L. Rosenberg (2013), The Tauern Window (Eastern Alps. Austria): A new tectonic map, with cross-sections and a tectonometamorphic synthesis, *Swiss J. Geosci.*, *106*, 1–32, doi:10.1007/s00015-013-0123-y.

Schneider, S. (2014), Exhumation mechanisms of middle and lower crust in the western Tauern Window, Eastern Alps PhD thesis, Freie Universität Berlin, 167 pp.

Schneider, S., K. Hammerschmidt, and C. L. Rosenberg (2013), Dating the longevity of ductile shear zones: Insight from $^{40}Ar/^{39}Ar$ in situ analyses, *Earth Planet. Sci. Lett.*, *369–370*, 43–58, doi:10.1016/j.epsl.2013.03.002.

Schneider, S., K. Scharf, C. L. Hammerschmidt, A. Rosenberg, A. Gerdes, D. Frei, and A. Bertrand (2015), U–Pb ages of apatite in the western Tauern Window (Eastern Alps): Tracing the onset of collision-related exhumation in the European plate, *Earth Planet. Sci. Lett.*, *418*, 53–65, doi:10.1016/j.epls.2015.02.020.

Schuster, R., F. Koller, V. Hoeck, G. Hoinkes, and R. Bousquet (2004), Metamorphic structure of the Alps: Eastern Alps, *Mitt. Öster. Min. Ges.*, *149*, 175–199.

Selverstone, J. (1985), Petrologic constraints on imbrication, metamorphism, and uplift in the SW Tauern Window, Eastern Alps, *Tectonics*, *4*, 687–704, doi:10.1029/TC004i007p00687.

Selverstone, J. (1988), Evidence for east-west crustal extension in the Eastern Alps: Implications for the unroofing history of the Tauern Window, *Tectonics*, *7*, 87–105, doi:10.1029/TC007i001p00087.

Selverstone, J., G. Franz, S. Thomas, and S. Getty (1992), Fluid variability in 2 GPa eclogites as an indicator of fluid behavior during subduction, *Contrib. Mineral. Petrol.*, *112*, 341–357, doi:10.1007/BF00310465.

Staufenberg, H. (1987), Apatite fission-track evidence for postmetamorphic uplift and cooling history of the eastern Tauern Window and the surrounding Austroalpine (Central Eastern Alps, Austria), *Jahrbuch der Geol. Bundesanst.*, *130*, 571–586.

Steck, A. (2008), Tectonics of the Simplon massif and Lepontine gneiss dome: Deformation structures due to collision between the underthrusting European plate and the Adriatic indenter, *Swiss J. Geosci.*, *101*, 515–546, doi:10.1007/s00015-008-1283-z.

Steenken, A., S. Siegesmund, T. Heinrichs, and B. Fügenschuh (2002), Cooling and exhumation of the Rieserferner Pluton (Eastern Alps), *Inter. J. Earth Sci.*, *91*, 799–817, doi:10.1007/s00531-0020260-4.

Steininger, F. E., F. Rögl, P. Hochuli, and C. Müller (1989), Lignite deposition and marine cycles. The Austrian lignite deposits—A case history, *Sitzungsber. Akad. Wiss., Wien, Math.-Naturwiss. Kl.*, *197*, 309–332.

Stöckhert, B. (1984), K-Ar determinations on muscovites and phengites from deformed pegmatites, and the minimum age of Old Alpine deformation in the Austridic basement to the south of the western Tauern Window (Ahrn Valley, Southern Tyrol, Eastern Alps), *N. Jb. Miner. Abh.*, *150*(2), 103–120.

Stöckhert, B., M. R. Brix, R. Kleinschrodt, A. J. Hurford, and R. Wirth (1999), Thermochronometry and the microstructures of quartz—A comparison with experimental flow laws and predictions on the temperature of the brittle-plastic transition, *J. struct. Geol.*, *21*, 351–369, doi:10.1016/S0191-8141(98)00114-X.

Thöni, M. (1999), A review from geochronological data from the Eastern Alps, *Schweiz. Mineral. Petrogr. Mitt.*, *79*, 209–230.

Viola, G., N. S. Mancktelow, and D. Seward (2001), Late Oligocene-Neogene evolution of Europe-Adria collision: New structural and geochronological evidence from the Giudicarie fault system (Italian Eastern Alps), *Tectonics*, *20*, 999–1020, doi:10.1029/2001TC900021.

Von Blanckenburg, F., I. M. Villa, H. Baur, G. Morteani, and R. H. Steiger (1989), Time calibration of a PT-path from the Western Tauern Window, Eastern Alps: The problem of closure temperatures, *Contrib. Mineral. Petrol.*, *101*, 1–11, doi:10.1007/BF00387196.

Wagner, R., C. L. Rosenberg, M. R. Handy, C. Möbus, and M. Albertz (2006), Fracture-driven intrusion and upwelling of a mid-crustal pluton fed from a transpressive shear zone: The Rieserferner pluton (Eastern Alps), *Geol. Soc. Am. Bull.*, *118*, 219–237, doi:10.1130/B25842.1.

Wang, X., and F. Neubauer (1998), Orogen-parallel strike-slip faults bordering metamorphic core complexes: The Salzach-Enns fault zone in the Eastern Alps, *J. Struct. Geol.*, *20*, 799–818, doi:10.1016/S0191-8141(98)00013-3.

Wernicke, B. (1985), Uniform-sense normal simple shear of the continental lithosphere, *Can. J. Earth Sci.*, *88*, 108–125, doi:10.1139/e85-009.

Willett, S. D., and M. T. Brandon (2002), On steady states in mountain belts, *Geology*, *30*, 175–178, doi:10.1130/0091-7613(2002).

Wölfler, A., C. Dekant, M. Danisìk, W. Kurz, I. Dunkl, M. Putis, and W. Frisch (2008), Late stage differential exhumation of crustal blocks in the central Eastern Alps: Evidence from fission-track and (U-Th)/He thermochronology, *Terra Nova*, *20*, 378–384, doi:10.1111/j.1365-3121.2008.00831.x.

Wölfler, A., K. Stüwe, M. Danisik, and N. J. Evans (2012), Low temperature thermochronology in the Eastern Alps: Implications for structural and topographic evolution, *Tectonophysics*, *541–543*, 1–18, doi:10.1016/j.tecto.2012.03.016.

Wölfler, A., W. Frisch, H. Fritz, M. Danisik, and A. Wolfler (2015), Ductile to brittle fault zone evolution in Austroalpine units to the southeast of the Tauern Window (Eastern Alps), *Swiss J. Geosci.*, *108*, 239–251, doi:10.1007/s00015-015-0193-0.

Yamada, R., T. Tagami, S. Nishimura, and H. Ito (1995), Annealing kinematics of fission-tracks in zircon: An experimental study, *Chem. Geol.*, *122*, 249–258, doi:10.1016/0009-254(95)00006-8.

Yin, A. (1989), Origin of regional, rooted low-angle normal faults: A mechanical model and its tectonic implications, *Tectonics*, *8*, 469–482, doi:10.1029/TC008i003p00469.

Yin, A. (2004), Gneiss domes and gneiss dome systems, in *Gneiss Dome in Orogeny*, edited by D. L. Whitney, C. Teyssier, and C. S. Siddoway, *Geol. Soc. Am. Spec. Pap.*, 380, 1–14, doi:10.1130/0-8137-2380-9.1.